Stockholm University

Master Thesis

Degree Project in
Geology 60 hp

Thermal structure of a paleo-subduction zone (Dora-Maira Massif, Western Alps)

William Westin

Stockholm 2022

Department of Geological Sciences
Stockholm University
SE-106 91 Stockholm

Abstract

The Supervisor for the project is Paola Manzotti and the co-supervisor is Federica Schiavi.

In the Western Alps on the Italian side in the area of the Dora-Maira Massif five different tectonic units are investigated to get estimations on peak temperatures. The units that will be investigated from top to bottom is the Raccias Unit, Serre Unit, Chasteiran Unit, Sanfront-Pinerolo Unit. In this study, Raman spectroscopy technique will be used on 16 samples gathered in the field or provided. The mineral used in the Raman spectroscopy is the mineral graphite. This mineral is analyzed in order to estimate the maximum temperature registered by the different units. The Pinerolo Unit is especially interesting due to this unit have only estimated temperatures in the southern part and not in the northern part. Raccias Unit is also of high interest due to this unit is considered to be a high-pressure unit. The results of Raman spectroscopy indicate that peak temperature in the studied area increases from the lower to the upper units with a low difference from 480ºC to 568ºC. Where the Pinerolo Unit are homogenic and the Raccias Unit is in the lower part of the temperature spectra.

Table of Contents

Introduction

When a mountain chain is formed, there has been thickening of the crust by stacking continental and/or oceanic slices. Crustal thickening happens along a convergent plate boundary. On a convergent plate boundary, the process will move down rocks into great depth and then exhume them from a great depth to the surface. When the mountain chain is formed a thermal perturbation will develop as well. The typical temperature gradient for mountain belt is high temperature in the internal parts and towards the external parts it is gradually decreasing (Engi et al 2004). This is because the thickest part of the crust will be located in the internal part of the mountain belt. The radioactive minerals will be concentrated in the internal parts and therefore the largest amount of radioactive heat will be in the internal part of the belt (Engi et al 2004). This pattern has been recorded by Engi et al (2004) in the Central Alps.

Once a rock is exhumed, one can sample and study it in order to establish its pressure and temperature history. There are many different methods to estimate the maximum burial depth, and some are more complicated than others.

A widely used technique is to look at the mineral paragenesis (i.e. what minerals the sample contains, and are thought to be in equilibrium, and what is their composition). From such data, the maximum burial depth could be established.

If a more precise temperature estimation is required, one is better off looking at specific minerals. One of the commonly used method is the progressive transformation of organic matter into graphite. With increasing temperature, the ordered, crystalline, state is better and better achieved. By shooting a laser beam on a single graphite crystal, one can estimate the ordering state of the crystal using the Raman spectrometer. So, by knowing how much imperfections there is in the crystal, one can estimate the maximum temperature. There is also a limit to this method due to the fact that graphite will be perfectly ordered above c. 650 ^{o}C.

This study will investigate the potential thermal gradient in the northern Dora-Maira Massif (Western Alps) by applying Raman spectroscopy on carbonaceous material on a set of samples.

The Alps

An introduction and a general overview

The *Alps* are a mountain belt located in Central-Southern Europe extending across eight different countries for a total length of ~1200 km (Agard 2021). The highest peak is the Mont Blanc (4810 m), a wonderful mountain mainly made of Permian undeformed granites (Gallach et al 2021) located at the French-Italian border that every year attracts thousands of climbers and hikers.

The Alps are not only a place well-known for stunning landscapes where people go on holydays to ski or hike, but they are a natural laboratory for understanding a wide range of geological processes (e.g. climate change, glacier retreat, uplift and erosion on the mountain topography; orogenic dynamics; seismicity). Indeed, the Alps exposes at the surface rocks then were buried (subducted) at great depth: their study helps to understand how mountain belts are built.

The Alps results from the closure and subsequent subduction of two small Jurassic oceanic basins (i.e. the Piemonte-Liguria Ocean and Valais Ocean, (Manzotti et al 2021; Vialon 1966; Decrausaz et al 2021). These two oceanic basins did not exceed 300-400 km and 50-200 km, respectively (Le Breton et al. 2020; Agard and Handy 2021). Due to the small size, the Valais Basin didn't get an active spreading ridge like the Piemonte-Liguria Ocean (Pfiffner 2014). The closure of these oceanic basins was followed by collision between the European and Adriatic plates (Pfiffner 2014). In the Alps, subduction of oceanic and continental crust occurred over a range of 50-60 million years (Ma) from 100-85 Ma to 40-35 Ma with a minimum rate of convergence of about 6.6-7 cm/y (Agard and Handy 2021).

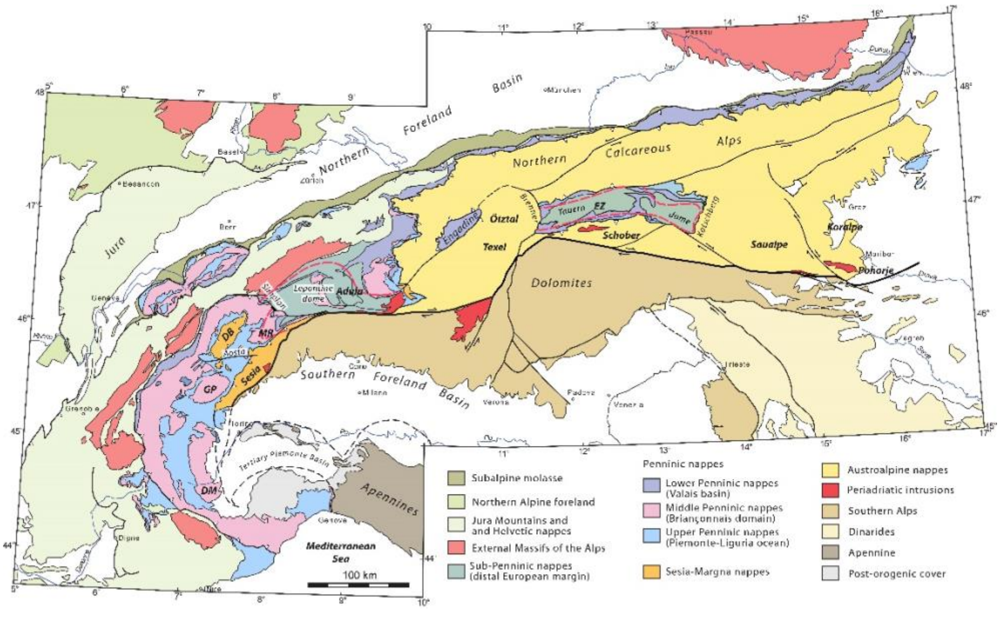

Figure 1. Tectonic map of the Alps (Manzotti and Ballèvre 2022; redrawn from Schmid et al. 2004).

The *Western Alps* exposes oceanic and continental crust that were deeply buried (at depth higher than 60-100 km). In this portion of the belt, the exceptional preservation of metamorphic rocks that equilibrated at high pressure low temperature (HP-LT) conditions (blueschist-facies: e.g. Queyras (Lagabrielle et al 2015) to quartz eclogite-facies: e.g. Gran Paradiso Massif (Manzotti et al. 2015) and even at ultra-high pressure (UHP) conditions (coesite-eclogite facies: Lago di Cignana Unit and Brossasco-Isasca Unit (Reinecke 1991; Chopin et al. 1984) is due to the lack of a collision-related metamorphic (amphibolite-facies) overprint. This metamorphic overprint is present in the Central Alps and HP and UHP rocks are therefore less abundant in the Central and Eastern Alps (Bachmann et al. 2009; Angiboust et al. 2009). Here, the increase in temperature associated with collision produced the development of a Barrovian metamorphic overprint at 35-30 Ma (the Oligocene "Lepontine Dome", (Handy et al 2010).

My master thesis in the framework of the Alpine belt

To sum up, the Alps are a worldwide known place for geologists. In the past, it was a source of inspiration for the birth of the plate tectonic theory (e.g. Trumpy 1990; McCarthy el al 2020) and they are today investigating to solve a wide range of geological problems and the answer to enigmatic and intriguing scientific questions, such for example the lack of a magmatic arc (see McCarthy et al 2020 for a recent possible explanation about this topic). For all these reasons, the Alps have been and will continue to be studied through generations. Amongst the other studies, my master thesis seeks to reconstruct the large-scale thermal structure of the palaeo-subduction zone in the Western Alps, quantifying the peak metamorphic temperatures reached by different tectonic units. This will be achieved using Raman Spectroscopy of Carbonaceous Material thermometry (Beyssac et al. 2002) on metamorphic rocks collected along a complete transect across the Western Alps.

The temperature history of these rocks will provide a direct snapshot on the thermal structure of past and modern subduction zones on Earth and an exceptional basis for understanding how difference in temperature across a mountain belt relate to specific tectonic processes, including implications for the location and mechanisms of earthquakes (seismicity).

Geology of the Southern-Western Alps

This study focuses on the SW Alps, an area world-wide known for spectacular HP metamorphic rocks (Figures 2 and 3). Overall, the distribution of mineral assemblages in the Western Alps indicates increasing metamorphic P–T conditions from the westernmost to the easternmost units (Tajčmanová et al. 2021). In this area, the nappe stack comprises from top to bottom:

1) Continental rock units consisting of the continental-landmass Briançonnais in-between the Valais ocean and Piemonte-Liguria ocean
2) Oceanic units derived from the Piemonte-Liguria ocean (Queyras and Viso)
3) Basement rocks that crops out as tectonic window below the Piemonte-Liguria Ocean. They are the Dora-Maira, Gran Paradiso and Monte Rosa nappes and they are also

known as Internal Crystalline Massifs (Ballèvre et al. 2020). This study focuses on the Dora-Maira Massif (Fig. 2)

Because the area of study exposes the basement rocks of the Dora-Maira Massif and remnants of the Piemonte-Liguria Ocean, the following sections will focus on these domains.

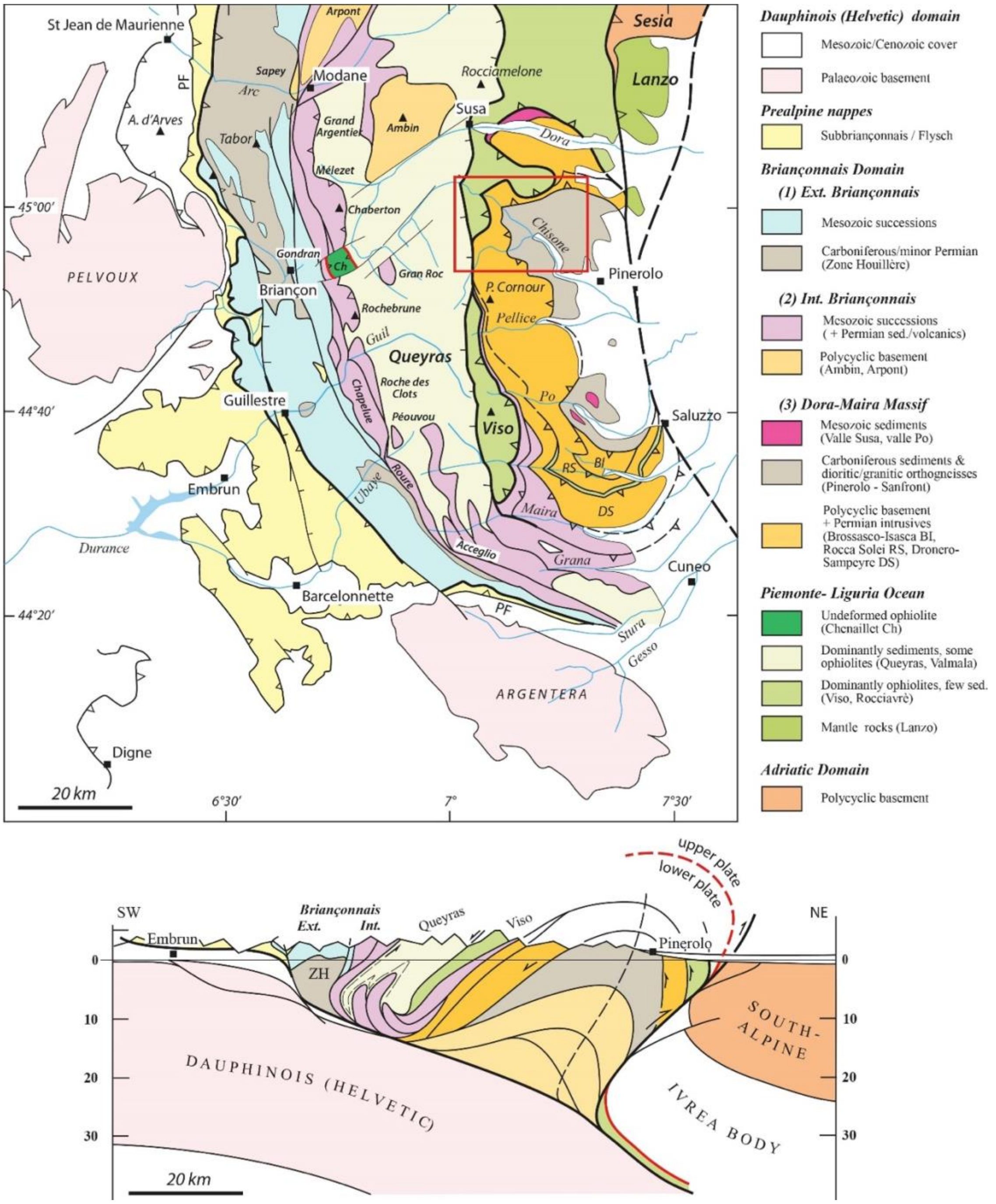

Figure 2. Simplified geological map of the SW Alps, showing the location of the studied area in the Dora-Maira Massif (modified after Ballèvre et al. 2020). The red square indicates the area of study. The crustal-scale cross-section shows a potential interpretation of the structures at depth (Ballèvre et al. 2020).

Piemonte-Liguria Ocean

Tectonic units derived from the Piemonte-Liguria Ocean may be divided into two main types (Agard 2021):

1) Units dominated by sediments with a few ophiolite complexes (called S-type units)
2) Units mainly made of serpentinites (formerly exhumed mantle) associated with meta-gabbros and meta-basalts with few sediments (called MUM-type units).

This lithological distinction is associated with a difference in the Alpine metamorphism. The S-type units reached low-grade blueschist-facies condition (e.g. Manzotti et al. 2021), whereas the MUM-type units are characterized by high-grade blueschist and eclogite facies (Bousquet et al. 2012; Agard 2021). In the SW Alps, where my study focuses, the Queyras is an example of the S-type unit whereas the Viso Unit is an example of the MUM-type unit.

The *Queyras Unit*

The Queyras Unit is located in the southern Western Alps (Figs 2 and 3). It consists of Upper Cretaceous calcschist and lower Cretaceous metapelites with minor mafic-ultramafic slices (Herviou et al. 2021). In the Queyras Unit, from west to east a continuous increase in metamorphic grade from ~ 12 kbar ~ 300 °C to ~20 kbar ~480 °C has been established (Bousquet et al. 2008, Agard et al. 2021)). The metamorphic grade of the area is considered to be peaking at upper blueschist-facies (Schwartz et al. 2000, Goffé et al. 2004, Michard et al. 2004).

The Viso Unit

The Viso Unit is mostly composed of eclogitic facies meta-ophiolites and it is well exposed in the area of the Viso Mountain (Messiga et al 1999, Angiboust et al. 2012). The Viso Unit contains one of the largest slices of oceanic lithosphere among the Piemonte-Liguria Ocean (Lombardo et al 2002). The meta-ophiolite provides well-preserved fragments of Tethyan oceanic lithosphere, with recognizable lithostratigraphic successions. The P-T conditions of the Viso Unit occurred at 20-26 kbar and 480- 580 °C (Messiga et al 1999, Schwartz et al 2000, Castelli et al 2002, Groppo et al 2010, Angiboust et al 2012). The age of the peak P-T conditions is 45-46 Ma (Duchêne et al 1997).

In the studied area, remnants of eclogite-facies oceanic rocks are discontinuously exposed. One of these slices is located in the area of a mountain called Raccias. Such oceanic rocks in the studied area are hereafter referred to as Raccias Unit.

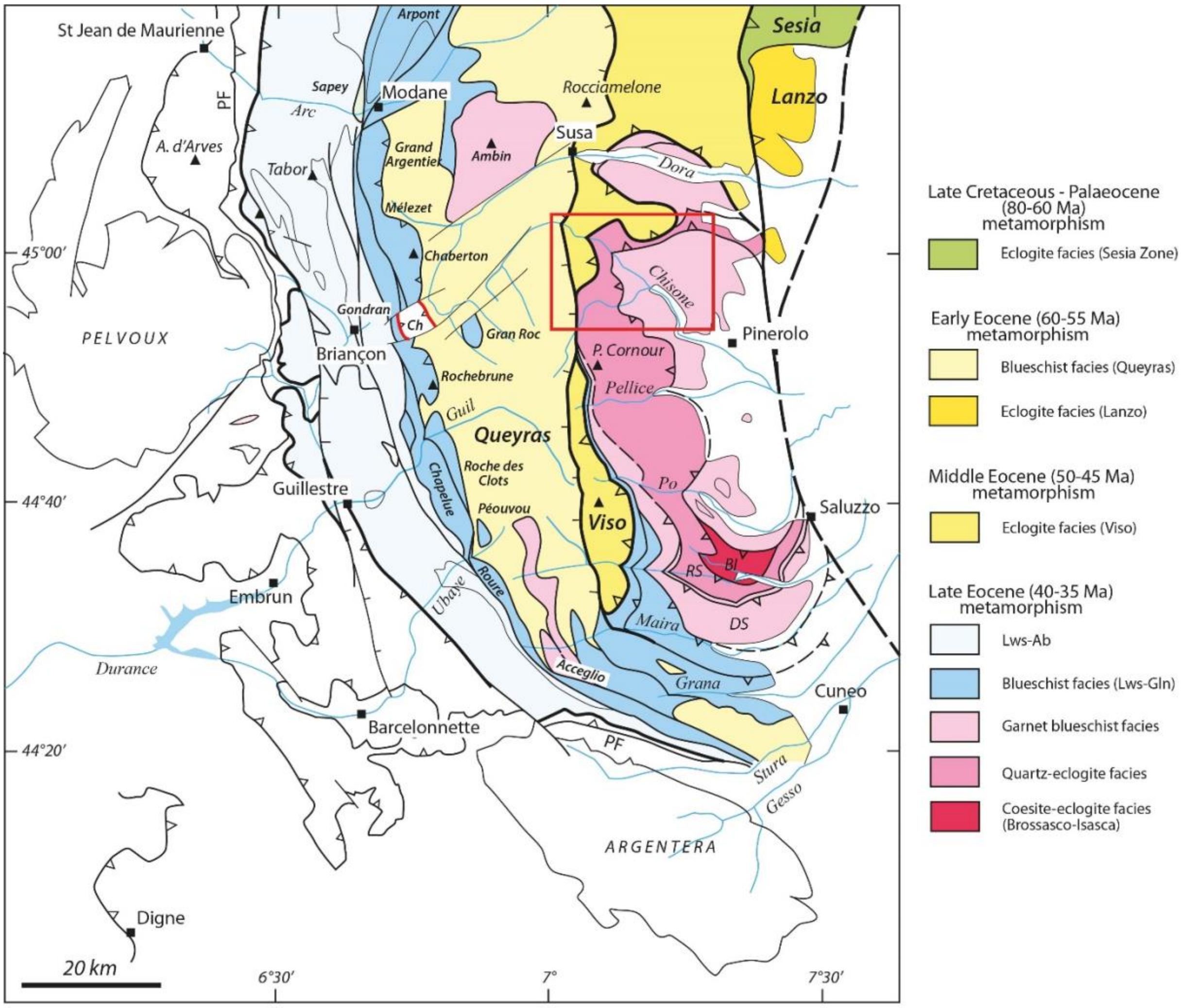

Figure 3. Simplified metamorphic map of the SW Alps. Colours refer to both metamorphic grade (in terms of metamorphic facies) (from Ballèvre et al. 2020).

The Dora-Maira Massif

The Dora-Maira (DM) Massif is one of the Internal Crystalline Massifs in the Western Alps (Figs 2 and 3) and before the Alpine orogeny it was part of a microcontinent called Briançonnais (Schmid et al 2004). It has an elliptical shape and extends over an area of 1750 km2 (Sandrone et al 1993). It comprises different tectonic units made of Palaeozoic basement. These units registered Alpine metamorphic conditions that range from blueschist- to eclogite-facies.

In the following, I will detail the geology of the northern Dora-Maira Massif, where my study focuses.

In this area, from bottom to top, the following units constitute the Dora-Maira Massif:

- *The Sanfront-Pinerolo Unit (PU)*

  It is the deepest unit exposed in the Dora-Maira Massif and together with the Money Unit represents the deepest structural level observed in the nappe stack (Manzotti et al. 2015; Manzotti et al 2016). It is discontinuously exposed from the Po valley in the south to the Sangone valley in the north.

It consists of metasediments (mainly micaschist interlayered with minor paragneiss) Carboniferous in age (Manzotti et al 2016) intruded by Permian granites and diorites (e.g. Freidour granite and Malanaggio diorite; Bussy and Cadoppi 1996).

One of the first geologists that explored the Pinerolo Unit was Novarese (1885, 1898, 1905) during the compilation of the geological map of Italy (i.e. "Carta Geologico d'Italia"). In the explanatory notes of the map, Novarese (1898, 1905) reported the extremely high content of carbonaceous material (hereafter referred to as graphite) present in the micaschists and provided a detailed description of the main graphite sites. In the northern Pinerolo Unit, more precisely in the Germanasca valley, several graphite mines were active from 1835 to 1984 (Bounous 2018). The anthracite extracted from these mines were considered one of the purest at that time. In the micaschist from the Pinerolo Unit, Novarese (1895) also reported the local presence of garnet and chloritoid (1895), two minerals that have been later found also by Vialon (1966).

There are no P-T estimates for the northern sector of the Sanfront-Pinerolo Unit and therefore the Alpine metamorphic evolution of this area is still unknown. In the southern part, P-T conditions of 14-16 kbar 400-500 °C (Avigad et al. 2003) or 20-23 kbar 500-515 °C (Groppo et al. 2019) have been estimated for this unit.

- *The Chasteiran Unit*

The Chasteiran Unit consists of garnet-chloritoid micaschist and equilibrated at *UHP* metamorphic conditions during the Alpine orogeny (Manzotti et al. in press).

- *The Muret Unit*

The Muret unit (Nosenzo et al. 2022) consists of a Palaeozoic basement that registered a polycyclic evolution (i.e. Variscan and Alpine). The unit is manly composed of late Neoproterozoic to Ordovician meta-sediments intruded by a kilometre-scale early Silurian granodiorite body. This Silurian granodiorite is referred to as Muret orthogneiss (Nosenzo et al. 2022). The pre-Alpine Barrovian metamorphism occurred at 4-5 kbar ~500 oC to 6-7 kbar ~650 °C and is dated at 324 ± 6 Ma by U-Th-Pb monazite (Nosenzo et al. 2022). The Alpine metamorphism of this unit reached eclogite-facies conditions and it is associated with the development of garnet, omphacite and rutile in meta-basalts (Borghi et al. 1985). Alpine peak P-T conditions of 9-14 kbar ~ 500 °C (Pognante and Sandrone 1989) have been estimated for the Muret Unit.

- *The Serre Unit*

The Serre Unit comprises felsic gneisses and associated volcano-sedimentary successions considered to be Permian in age and remnants of a dismembered Mesozoic cover (dolomites, marbles with subordinate calcschists and ankerite micaschists).

Methods

Fieldwork

Fieldwork was executed in three weeks, from 30th of August to the 21th of September. The people who were in the field with me was Francesco Nosenzo, Paola Manzotti, Michel Ballèvre and three of the days we were joined by Stefan M. Schmid, a structural geologist from ETH (Zurich, Switzerland).

In the field notes of visual information (e.g. structural measurements, note-observations, sketches, GPS position, photos) were taken to get a better understanding of the area. In addition, rock-samples containing graphite were collected. In the field an old abandoned graphite mine was visited to gather notes of historical and visual information. The rock samples gathered in the field was sent away to Italy and France to make thin sections.

The aim of the fieldwork was to get a better understanding of the structure of the Dora-Maira Massif in the studied area and to get a first perspective of the geological history of the Alps.

Petrographic observations

I have investigated 16 samples in thin sections for petrographic observations. I identified the minerals present in the different samples and estimated their abundance. I recognised and described the main structural elements (e.g. foliations) and the minerals that define the foliation. Preparation for the Raman analysis was also done with the optical (petrographical) microscope. This was done by identifying graphite-rich areas in thin section and mark it by drawing a circle around these areas with a pencil.

Raman spectroscopy on carbonaceous material

Raman spectroscopy on carbonaceous material is a well-known geothermometer (Beyssac and Lazzeri, 2012). This technique works by focussing a laser-beam on a graphite crystal: the laser photons hit and interact with molecules in the crystal, so the molecules gain energy and are excited into a virtual energy state (Beyssac and Lazzeri, 2012). This energy state depends on the intensity of the laser (Beyssac and Lazzeri, 2012). The back-scattered photons are then captured by the lens, transmitted and dispersed through a spectrometer, and finally counted by a Charge Coupled Device (CCD) detector (Beyssac and Lazzeri, 2012) (fig 4). Most of the scattered light is at the same wavelength (energy and colour) as the laser source and does not provide useful information: this is called Rayleigh elastic scattering. However, a small amount of light (typically 0.0000001%) is scattered at different wavelengths (energies and colours), which depend on the chemical structure of the analyte: this is called inelastic Raman scattering, and this is what is used (Fenn et al 2011).

532 nm diode laser

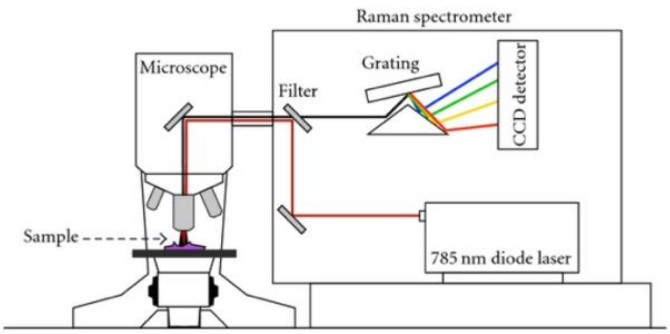

Figure 4. Typical setup for a Raman spectrometer with a near-infrared laser attached to a microscope (Fenn et al 2011). The figure is modified from the original figure from the paper of Fenn et al 2011.

The acquired Raman spectrum will look different depending on the crystal structure. During metamorphism, graphite crystallises at peak temperature and defects are progressively lost at increasing temperature (Beyssac et al. 2003). The degree of crystallinity of a phase is an indicator of how a crystal has been subjected to high temperature (Beyssac et al. 2003) and it increases at increasing temperature. This method can be applied on samples that reached a maximum temperature of 650 ^{o}C (Beyssac et al. 2002). This is because at this temperature a graphite crystal displays the highest degree of crystallinity (Beyssac et al. 2002).
The spectrum of a mineral analysed by Raman spectroscopy displays characteristic peaks. Graphite shows two main groups of peaks in two main regions of the spectrum, namely the first- and second-order regions (Beyssac et al. 2003). The first-order peak region is between 1100 and 1800 cm^{-1}, the second one is between 2200 and 3400 cm^{-1} (Beyssac et al. 2003). For Raman spectroscopy on carbonaceous material, the first order region is investigated. In this region, the first order peaks are located at ~1350 cm^{-1}, ~1580 cm^{-1} and ~1620 cm^{-1}. These peaks are called D1, G and D2, respectively (Beyssac et al. 2003) (fig 7). The height and the width (area) of the peaks are used to calculate the maximum (peak) temperature reached by a graphite crystal (Beyssac et al. 2002). To calculate the temperature, one needs to compare D1 against G, D1 and D2, by first calculating the ratio R2 = D1/(G+D1+D2) with D1, G and D2 representing the areas of those peaks (Beyssac et al. 2002), and then by applying the equation T = (- 445 * R2) + 641 (Beyssac et al. 2003). It is also good to calculate R1 (the variation of intensity ratio) and plot it against R2 to check the reliability of the data (Beyssac et al. 2002).

Analytical procedure for Raman measurements

Raman spectroscopy was used to analyse rock samples containing graphite, including both some provided samples and samples gathered in the field. The analysis was done at Université Clermont-Auvergne, Laboratoire Magmas et Volcans in France.

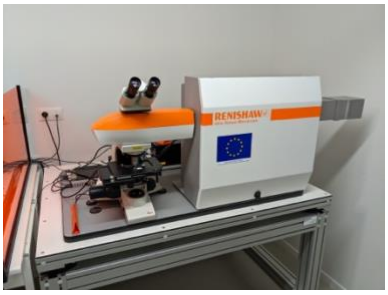

Figure 5. The Renishaw inVia confocal Raman micro-spectrometer used for the analysis.

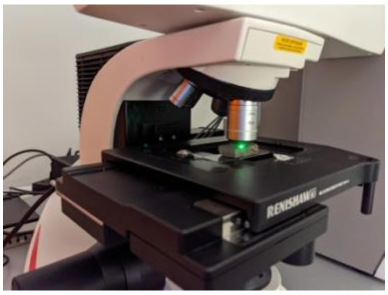

Figure 6. Close-up picture of the laser beam striking the sample during the analysis.

Raman spectra were acquired in back-scattered geometry using a Renishaw inVia confocal Raman micro-spectrometer equipped with a 532.1 ± 0.3 nm diode laser, a CCD detector of 1040 × 256 pixels, a Rayleigh rejection edge filter, and a Leica DM 2500M optical microscope with a motorised XYZ stage. During analysis, a grating of 2400 grooves mm^{-1}, a ×100 microscope objective, a 20-µm slit aperture and a < 3 mW laser power on the sample were used. Under these analytical conditions, the spectral resolution was ~ 0.4 cm^{-1}, while the lateral and vertical spatial resolutions were respectively 1 µm and 2-3 µm near the sample surface (fig 5-6). The laser was generally focused at 5-10 µm depth to analyze graphite located below mineral phases. The spectra were recorded using the WiRE^{TM} 4.4 software in the wavenumber range from ~ 900 to 2000 cm$^{-1,}$ containing the two principal vibrations of graphite. Each analysis consisted of 10 accumulations of 20 seconds each. Daily calibration of the spectrometer was performed using silicon (520.5 cm^{-1} peak) and diamond standards (1331.5 cm^{-1} peak).

The Raman spectra received is processed by baseline correction if needed, truncation if a diamond peak is in the spectra. When this is done the tool "peak fit" is used to make a perfect fit of the peaks that are calculated.

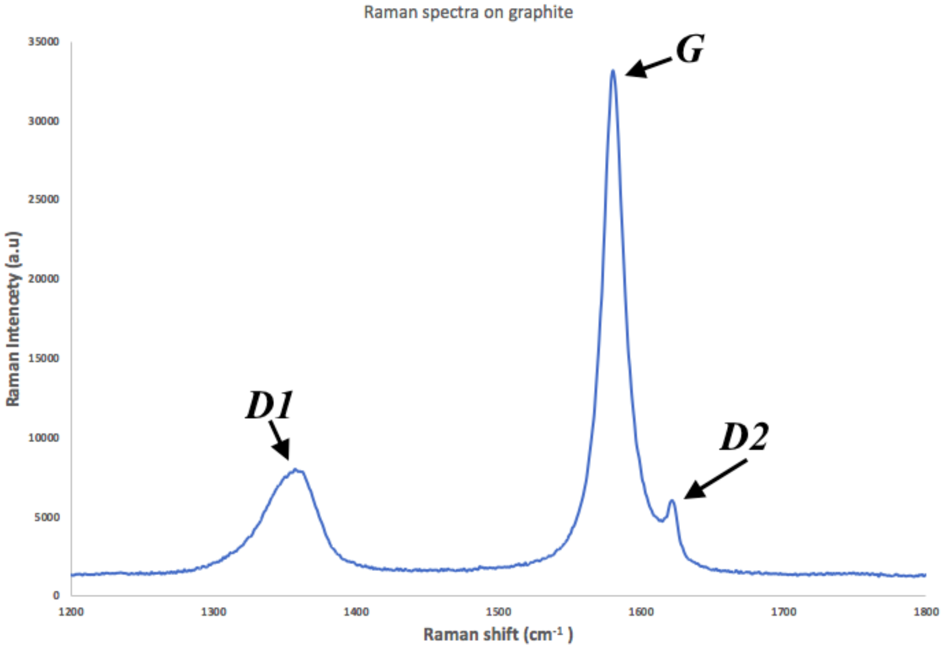

Figure 7. Raman spectrum from one graphite in the GM2029 sample.

Results

Fieldwork

Amongst the five investigated tectonic unit, the Pinerolo Unit is characterized by the highest amount of graphite. Graphite is found as dispersed material within the matrix of the meta-conglomerates and meta-sandstones, but it is also concentrated in cm- to m-thick layers. The latter are dark grey in color and in the past were mined. The old abandoned graphite mine (i.e. Garnier mine) that was visited where highly weathered and the mines was not safe to enter. Even though the mine was not entered the graphite layers have been seen at their entrance allowing a better understanding of their setting (fig 7a-b). Exploring the mine was not only for understanding the geology of the area, but it was also an occasion for place the mining activity in an historical perspective, i.e. how the graphite was mined and why the mines was no longer economically sustainable. The structural part in the field gave a good idea of how graphite-rich layers may be highly deformed and have acted as decollement layers (fig 8).

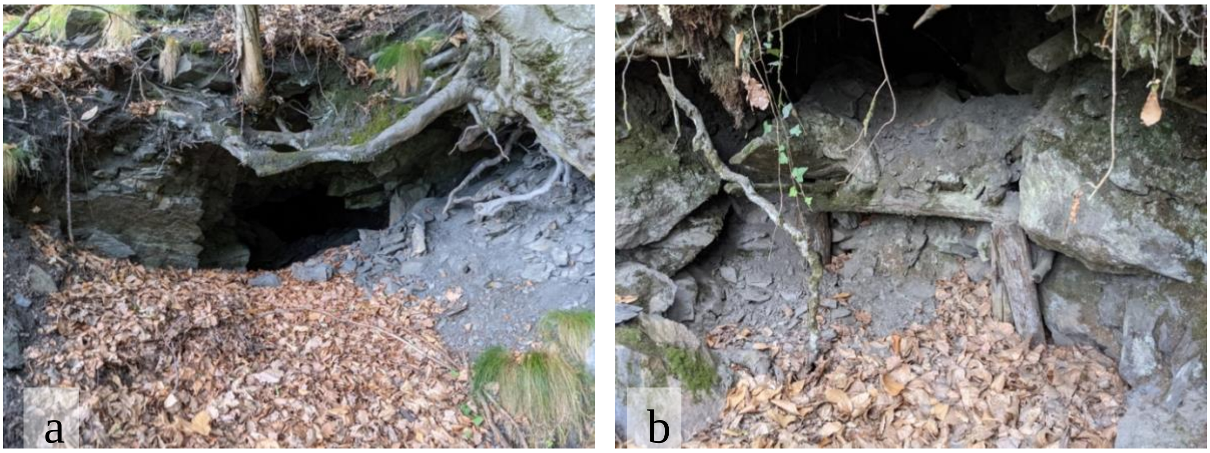

Figure 8. (a) A graphite mine has started to collapse, but the entrance is still intact. (b) A graphite mine with a collapsed entrance. Both of the mines are located in the Pinerolo Unit in the Dora-Maira Massif. We did not enter in both mines due to the high risk of collapse.

Figure 9. An example of a graphite layer at the contact with meta-sandstone (Pinerolo Unit). The soft graphite rich layer is deformed and worked at a shear plane.

Petrography of the studied samples

Eighteen thin sections have been studied by optical microscopy. The studied samples were collected in the different Units exposed in the northern Dora-Maira Massif. From bottom to top (i.e. from the west to east) these units are: the Sanfront-Pinerolo, Chasteiran, and Serre Units. No samples have been investigated in the Muret Unit. This Unit recorded a polycyclic evolution (Nosenzo et al. 2022). Therefore, it is not possible to attribute the maximum temperature obtained by RSCM to the Alpine evolution.
Along the section, one sample from the oceanic eclogite-facies Raccias Unit (i.e. the equivalent of the Viso Unit) has also been investigated by optical microscopy and Raman spectroscopy.

Sanfront-Pinerolo Unit
Eight samples from the Sanfront-Pinerolo Unit have been analyzed. Seven samples were collected in the northern sector of the Unit (Germanasca, Chisone and Sangone valleys), whereas one sample (PO2081) was collected in the southern part of the Sanfront-Pinerolo Unit.

Northern sector

Pinerolo Unit

SN1902: Graphitic micaschist

Macroscopic aspect
Sample SN1902 is a dark micaschist due to the high graphite modal amount.
Deformation
In thin section, one main foliation (S_1) is pervasive and is gently microfolded. S_1 foliation is marked by quartz layers and mica-rich domains
Mineral composition
The mineral composition of the sample is graphite 40%, quartz 25%, white mica 13%, chlorite 7%. Accessory minerals (less than 2% each) include, Fe-rich oxide.
Timing of mineral growth with respect to deformation
The main minerals define S_1 foliation the largest quartz crystals contain inclusions of graphite.
Graphite abundance and distribution
Graphite is extremely abundant in this sample, and is dispersed in the whole sample, although it may be concentrated in some layers parallel to the foliation S_1. Highest concentrations of graphite are seen on both sides where the S_2 is cutting the S_1 parallel to the S_1 plane. Graphite is observed included in biotite, white mica, quartz, and less frequently in chlorite.

CH2003: Garnet-chlorite micaschist

Macroscopic aspect
Sample CH 2003 is a blackish-greyish micaschist with pinkish-reddish mm scale garnets.
Deformation
In thin section, two foliations are easily distinguished. The first one (S_1) is pervasive and is microfolded by open crenulations locally associated with the development of a second set of cleavage planes (S_2).
Mineral composition
The mineral composition of the sample is quartz 30%, chlorite 25%, white mica 20%, garnet 10%, ilmenite 5%, graphite 5%, titanite 5%. Accessory minerals (less than 2% each) include chloritoid, biotite, albite, epidote, pyrite and rutile.
Timing of mineral growth with respect to deformation
The crenulation foliation S_2 curves around garnet porphyroblasts, developing pressure shadows filled by quartz and chlorite. Garnet rarely includes chloritoid laths. These are heavily cracked, with chlorite and sometimes biotite growing into the cracks. Within the garnet crystals needlelike rutile crystals can be seen as inclusions, but the rutile crystals can be seen in the matrix as well. The garnet crystals are getting replaced by chlorite, some biotite and is altered along cracks by a yellowish product, possibly altered chlorite (fig 10).
The few albite crystals in the sample are replaced by epidote.
In some parts the foliation is also wrapping quartz crystals and albite.
Graphite abundance and distribution
Graphite is very abundant in this sample, and is dispersed in the whole sample, although it may be concentrated in some layers parallel to the foliation S_1. It is also more abundant along some of the S_2 planes. In such cleavage planes, tiny pyrite crystals are also defining the foliation. Graphite is observed included in garnet, white mica, quartz, and less frequently in chlorite. Not to be confused with graphite are other opaque minerals, seen as large plates parallel to the S_1, and attributed to ilmenite.

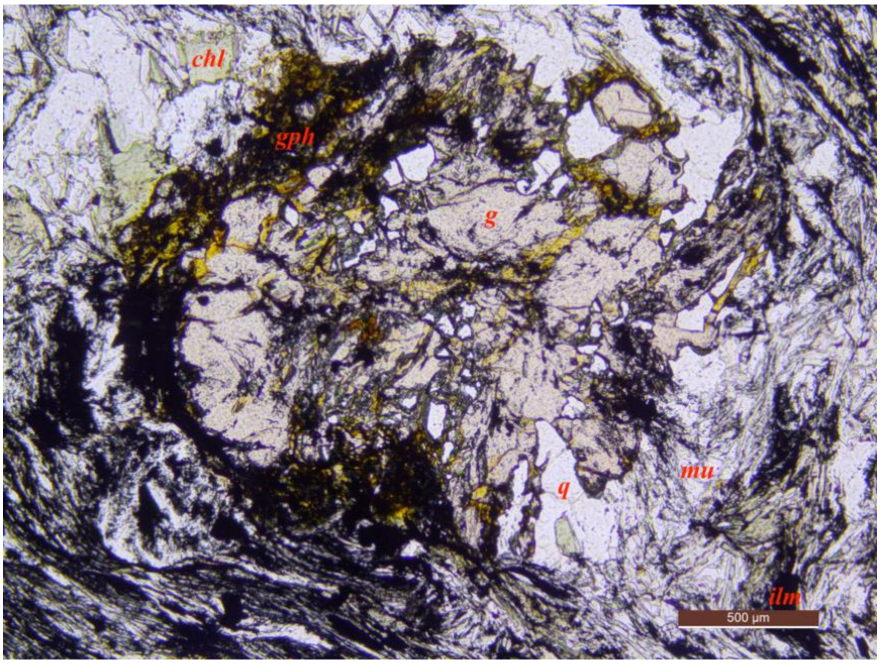

Figure 10. Chlorite and a yellowish alteration product are replacing the garnet, surrounded by high amounts of graphite.

GM1404b: micaschist

Macroscopic aspect
Sample GM1404b is a pale grey micaschist with mm size quartz veins.
Deformation
In thin section, one poorly defined foliation is present.
Mineral composition
The mineral composition of the sample is quartz 55%, albite 25%, white mica 8% and chlorite 7%. Accessory minerals (less than 2% each) graphite, ilmenite, titanite and garnet.
Timing of mineral growth with respect to deformation
Albite crystals displays an internal foliation defined by quartz, white mica, graphite and titanite. Albite also includes tiny idioblastic garnet crystals. The poorly-developed foliation wraps around albite porphyroblast and is defined by white mica and chlorite.
Graphite abundance and distribution
Graphite is not so abundant in this sample, but the graphite seen is dispersed in the whole sample, although it may be concentrated in some layers parallel to the foliation. Graphite are observed as inclusions in quartz, albite, and white mica.

GM1405a: micaschist

Macroscopic aspect
Sample GM1405a is a brownish-greyish micaschist.
Deformation
In thin section, one foliation can be recognized. It is defined by quartz lenses and mica-rich layers.
Mineral composition
The mineral composition of the sample is quartz 42%, albite 20%, chlorite 15%, white mica 5%, graphite 5 % and garnet 3%. Accessory minerals (less than 2% each) include biotite and ilmenite.
Timing of mineral growth with respect to deformation
The main foliation wraps around porphyroblasts of garnet and in some cases albite, developing pressure shadows filled by quartz, chlorite and white mica. Two types of garnet crystals are observed. Large garnet crystals are heavily cracked, with chlorite and sometimes biotite growing into the cracks (fig 11) and are strongly replaced by chlorite (frequently altered), less frequently by biotite. Tiny idioblastic garnet crystals are found as inclusions in albite. Ilmenite is dispersed in the matrix and is frequently associated with quartz and chlorite. Albite porphyroblasts displays tiny inclusions of garnet, quartz, white mica, chlorite, and graphite.
Graphite abundance and distribution
Graphite is quite abundant in this sample and the graphite seen is dispersed in the whole sample, although it may be concentrated in some layers parallel to the foliation. Graphite can be seen as inclusions in albite and in association with chlorite and quartz.

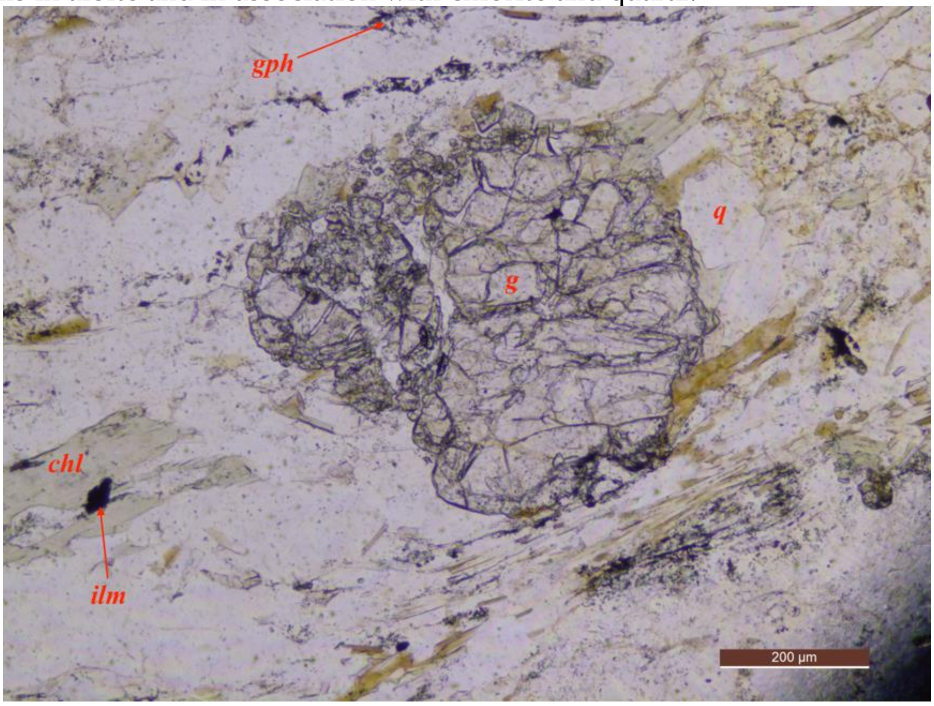

Figure 11. garnet is getting replaced by oxidized chlorite. Graphite is visible as inclusions in garnet, chlorite and quartz.

GM1419b: Graphitic micaschist

Macroscopic aspect
Sample GM1419b is a greenish-grey micaschist.
Deformation
In thin section, one poorly-developed foliation can be observed. It is marked by discontinuous layers of white mica and chlorite.
Mineral composition
The mineral composition of the sample is quartz 38%, chlorite 20%, white mica 15%, albite 5%, biotite 5%, graphite 4% and ilmenite 3%. Accessory minerals (less than 2% each) garnet, epidote, and tourmaline.
Timing of mineral growth with respect to deformation
Garnet crystals are broken in small pieces and partially dissolved. The garnet fragments are heavily cracked up and are replaced by chlorite (frequently altered), biotite (fig 12). Ilmenite can be observed in association with chlorite and biotite.
Graphite abundance and distribution
Graphite is not so abundant in this sample, but the graphite observed is dispersed in the whole sample, although it may be concentrated in some layers parallel to the foliation. Graphite can be seen as inclusions in chlorite, garnet and quartz.

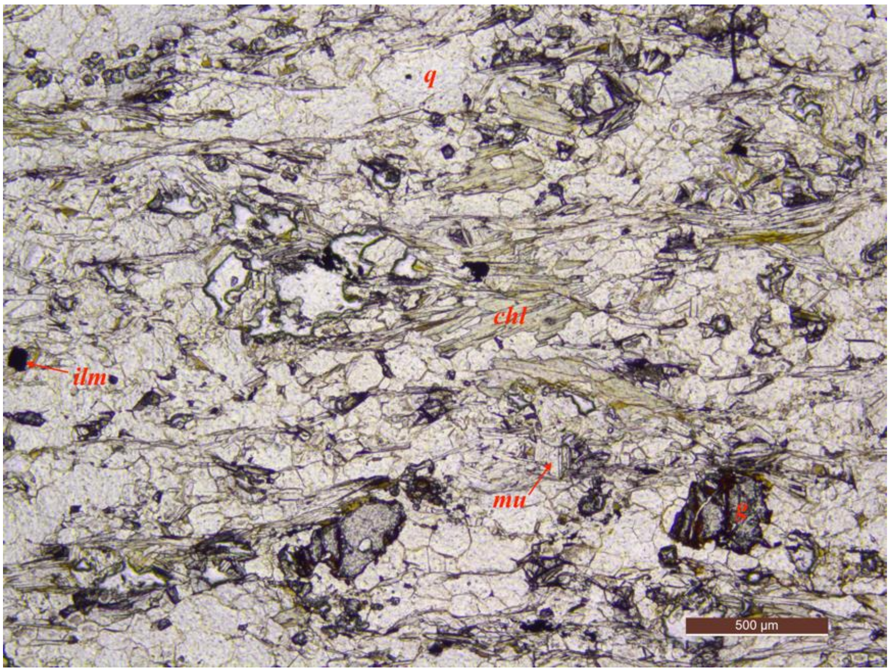

Figure 12. garnet in the image is bookend up and dispersed all over. Most of the mineral composition in the image is quartz.

GM1406a: Micaschist

Macroscopic aspect
Sample GM1406a is a greenish-grey micaschist with few mm sized black spots.
Deformation
In thin section, one well-developed pervasive foliation is present. This foliation is marked by quartz-layers, mica-rich domains. Albite porphyroblasts are stretched parallel to this fabric.
Mineral composition
The mineral composition of the sample is albite 30%, white mica 20%, chlorite 17%, quartz 15%, garnet 10% and ilmenite 6%. Accessory minerals (less than 2% each) graphite, epidote, carbonate, biotite, titanite and tourmaline
Timing of mineral growth with respect to deformation
Two types of garnet can be recognized in the sample. Garnet porpbyroblasts are broken in fragments. The latter are strongly fractured and partially dissolved. There are also partially replaced by chlorite (frequently altered), and minor biotite. Tiny idioblastic garnet crystals are dispersed in the rock (fig 13). Mm sized albite porphyroblast displays an internal foliation marked by white mica, titanite, graphite. This foliation is parallel to the main foliation in the matrix.
Graphite abundance and distribution
Graphite is not abundant in this sample but the graphite seen is dispersed in the whole sample, although it may be concentrated in some layers parallel to the foliation. Graphite is observed as inclusions in white mica, chlorite, albite, epidote and quartz.

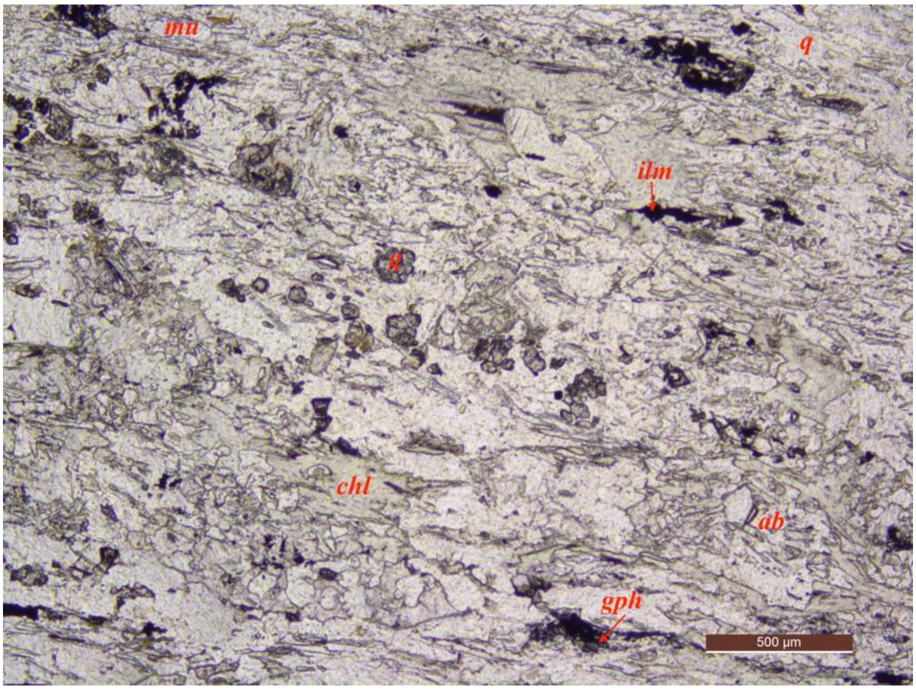

Figure 13. garnet in the image is bookend up and dispersed all over. The graphite in the sample is as seen in the image highly concentrated in some areas.

GM1908: Graphitic micaschist

Macroscopic aspect
Sample GM1908 is a greenish-grey micaschist with greyish-green spots.
Deformation
In thin section, the main foliation is defined by quartz layers and discontinuous white mica layers. This foliation is folded.
Mineral composition
The mineral composition of the sample is quartz 28%, chlorite 20%, white mica 15%, albite 5%, garnet 5%, ilmenite 5%, graphite 4% and biotite 4%. Accessory minerals (less than 2% each) tourmaline, epidote, and titanite.
Timing of mineral growth with respect to deformation
The rock contains tiny garnet crystals. At the rim, garnet is partially altered and displays brownish color (fig 14). Garnet contains unoriented inclusions of graphite. Albite porphyroblasts are strongly deformed by the folding event.
Graphite abundance and distribution
Graphite is abundant in this sample and the graphite seen is dispersed in the whole sample stretching parallel to the foliation. The graphite can be seen as inclusions in garnet, chlorite, quartz, biotite, chloritoid, white mica and tourmaline. Well preserved graphite crystals can be observed within the large quartz crystals.

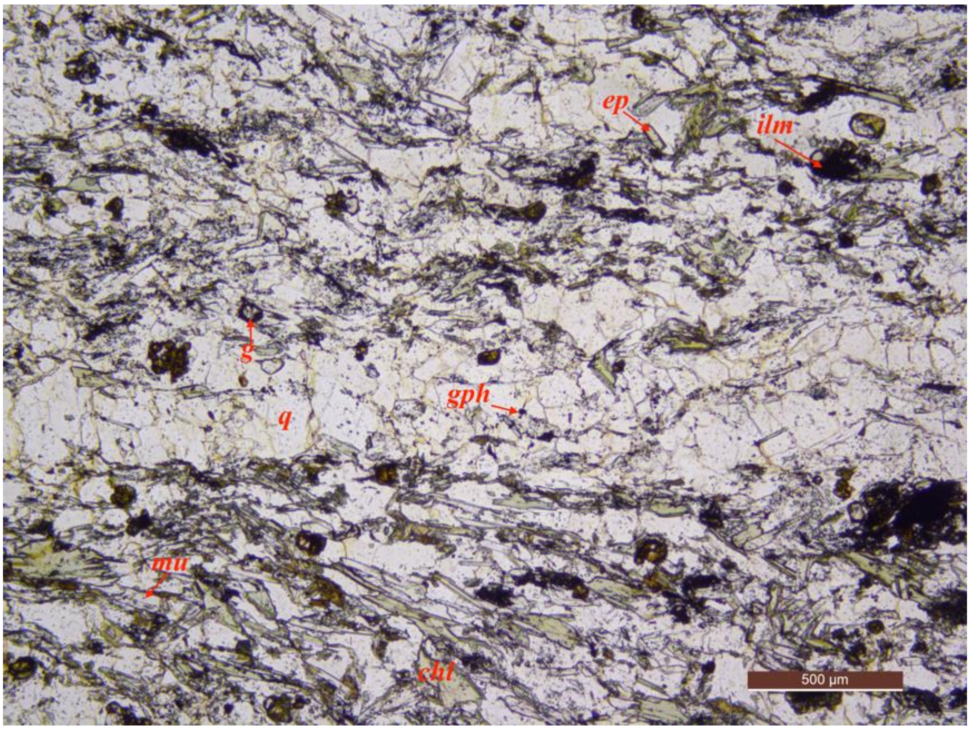

Figure 14. Graphite is gathered in to large clusters and quartz vein seen in the image is cutting through the whole sample.

CH1902: Graphitic micaschist

Macroscopic aspect
Sample CH1902 is a greenish micaschist.
Deformation
The rock displays a pervasive foliation marked by quartz bands and by mica-rich layers.
Mineral composition
The mineral composition of the sample is chlorite 35%, white mica 17%, albite 16%, quartz 13%, garnet 9%, ilmenite 4% and graphite 3%. Accessory minerals (less than 2% each) rutile, biotite, titanite, chloritoid and epidote.
Timing of mineral growth with respect to deformation
Big mm scale albite and garnet crystals are wrapped by the main foliation and display pressure shadows filled with chlorite, quartz and white mica. Garnet displays inclusions of rutile and quartz and is partially dissolved and replaced by chlorite and fine-aggregated of white mica (fig 15). Graphite and rutile occur as inclusions in albite porphyroblasts.
Rutile crystals in the matrix are replaced by ilmenite. Ilmenite is oriented parallel to the main foliation.
Graphite abundance and distribution
Graphite is abundant in this sample and the graphite seen is dispersed in the whole sample stretching parallel to the foliation. The graphite can be observed as inclusions in garnet, chlorite, quartz, white mica and in ilmenite.

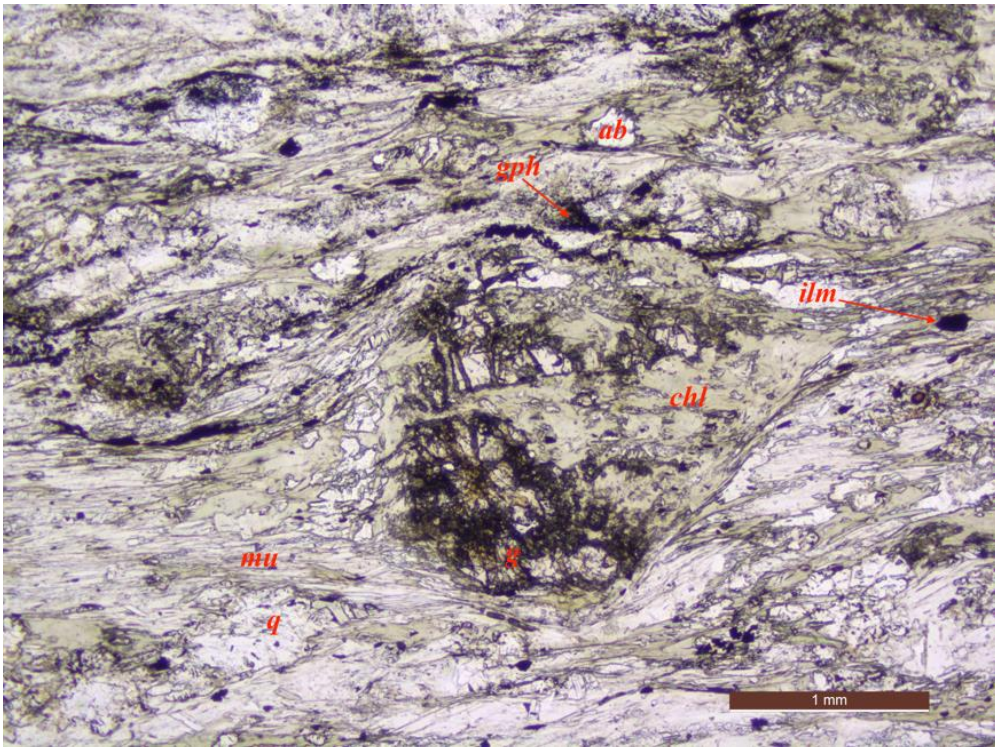

Figure 15. Chlorite in the image is replacing the garnet creating a pseudomorph. The foliation is bending around the pseudomorph.

Southern sector

PO2081: Graphitic micaschist

Macroscopic aspect
Sample PO2081 is a grayish-white with two distinct black spotted mm sized layers.
Deformation
A poorly defined foliation is marked by discontinuous thin layers of white mica, graphite and minor chlorite.
Mineral composition
The mineral composition of the sample is albite 35%, quartz 25%, graphite 15%, ilmenite 10%, chlorite 5%, white mica 3%. Accessory minerals (less than 2% each) rutile
Timing of mineral growth with respect to deformation
Albite porphyroblasts contains numerous inclusions of graphite, quartz, and minor white mica. Albite crystals display pressure shadows filled with mostly quarts and less frequently chlorite, white mica, ilmenite and graphite (fig 16).
Graphite abundance and distribution
Graphite is highly abundant in this sample, and is dispersed in the whole sample, although it may be concentrated in some layers parallel to the foliation. There is two 2-3mm wide layers with high graphite concentrated cutting through the sample. The graphite is getting concentrated in accompanying by crenulations. Graphite is observed as inclusions in albite, quartz, chlorite and white mica.

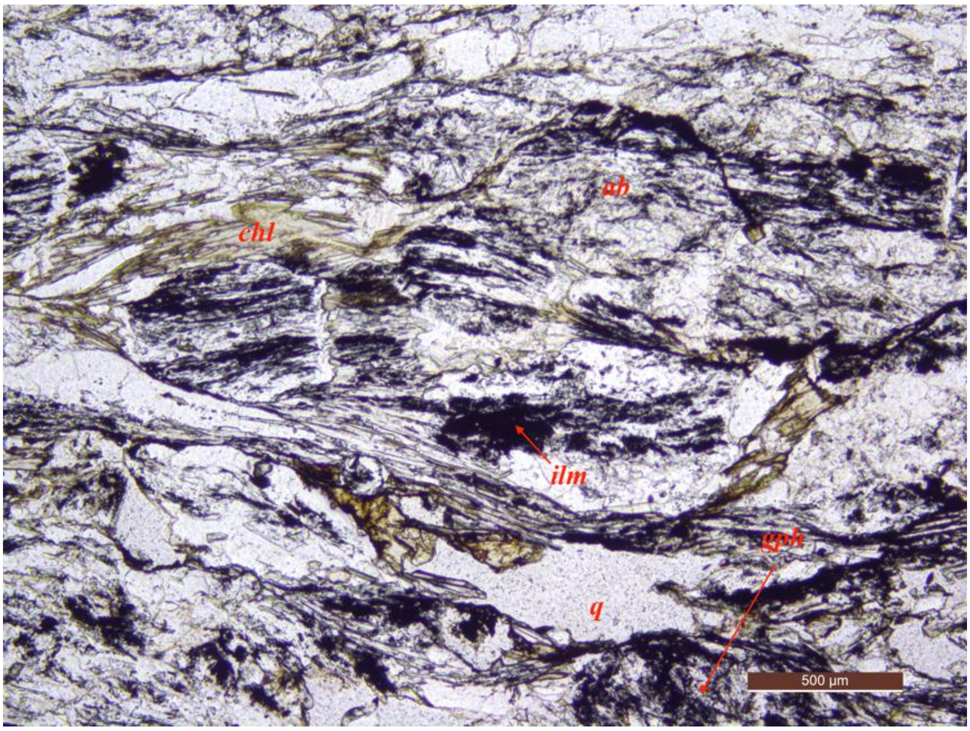

Figure 16. The large albite crystals in the image is bending the foliation and also creating a pressure shadow.

Chasteiran Unit

Three samples from the Chasterian Unit have been analyzed

CH1907-2: Garnet-chloritoid micaschist

Macroscopic aspect
Sample CH1907-2 is a grayish-green micaschist.
Deformation
In thin section, two foliations can be distinguished. The first and main one (S_1) is pervasive and is microfolded by open crenulations locally associated to the development of a second set of cleavage planes (S_2). S1 foliation is preserved in microlithons and is marked by the shape preferred orientation of chloritoid and white mica. The main foliation S2 is defined by quartz bands and by the shape preferred orientation of white mica and chloritoid. These two minerals are concentrated in layers.
Mineral composition
The mineral composition of the sample is white mica 35%, quartz 30%, chlorite 16%, chloritoid 6%, albite 4% and ilmenite 4%. Accessory minerals (less than 2% each) tourmaline, graphite, garnet, rutile and epidote.
Timing of mineral growth with respect to deformation
Chloritoid have inclusions of graphite and rutile. Chloritoid is zoned and displays light blue core and dark blue rim (fig 17). Chloritoid is sometimes partially replaced at the rim by chlorite. Chlorite is statically overgrowing the foliation and rutile is replaced by ilmenite.
Graphite abundance and distribution
Graphite is not so abundant in this sample, and is dispersed in the whole sample, although it may be concentrated in some layers parallel to the foliation. The graphite is observed as inclusions in chlorite, quartz, tourmaline, chloritoid and ilmenite.

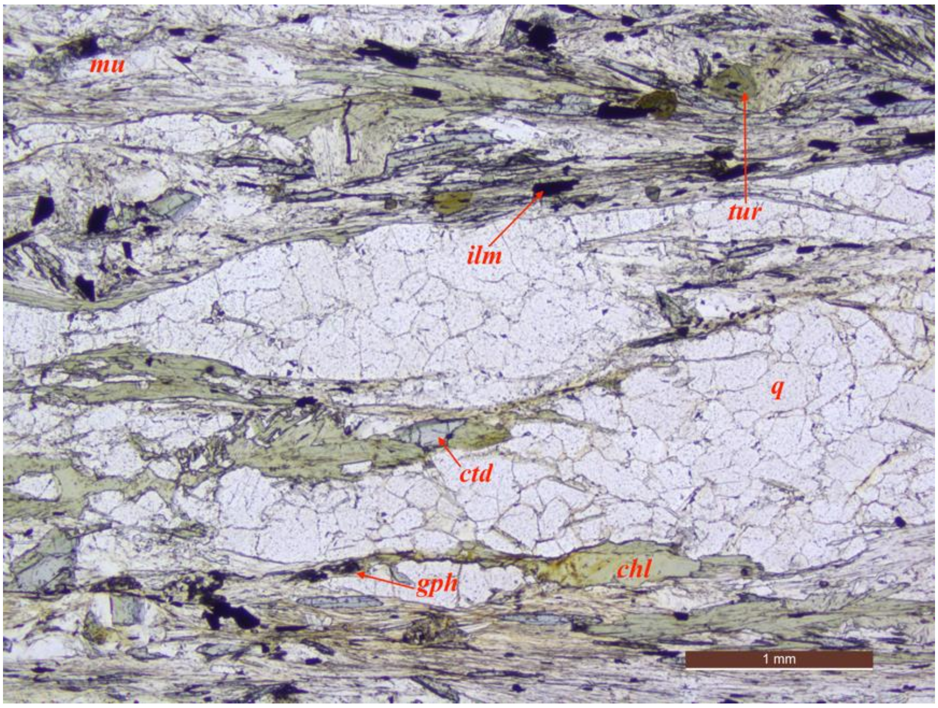

Figure 17. the large mm sized quartz vein in the image is cutting through the whole sample. Multiple colored chloritoid is seen getting replaced by chlorite.

GM2010: Garnet micaschist

Macroscopic aspect
Sample GM2010 is a pale gray micaschist with mm scale pinkish-white garnets.
Deformation
A main foliation is marked by quartz band and by mica-rich layers. This foliation is folded.
Mineral composition
The mineral composition of the sample is quartz 30%, white mica 25%, chlorite 20%, biotite 10%, albite 5% and garnet 5%, sodic amphibole 5%. Accessory minerals (less than 2% each) rutile, graphite, ilmenite and epidote.
Timing of mineral growth with respect to deformation
Large garnet crystals are wrapped by the main foliation (fig 19). Garnet contains a few inclusions of quartz and white mica. They are generally strongly fractured and replaced by chlorite at the rim and along fractures. Some of them are completely pseudomorphed by chlorite, biotite and albite. the chlorite is frequently oxidized. A few fine-grained aggregates consisting of chlorite and quartz are observed in the main foliation. They represent pseudomorphs after sodic amphiboles.
Graphite abundance and distribution
Graphite is not so abundant in this sample, and is dispersed in the whole sample, although it may be concentrated in some layers parallel to the foliation. Graphite is observed as inclusions in chlorite, biotite and quartz.

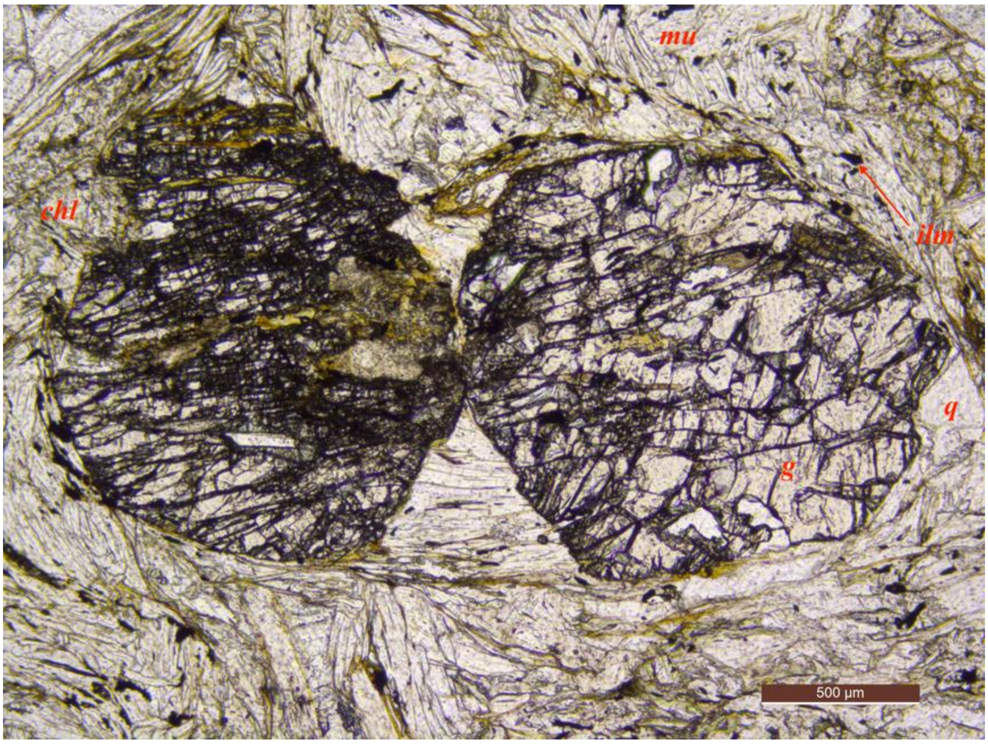

Figure 19. Two garnet crystals are highly fractures and are wrapped by the main foliation marked by white mica. Garnet crystals are partially replaced by chlorite.

Serre Unit

Four samples from the Serre Unit have been analyzed.

GM1904: Calcschist

Macroscopic aspect
Sample GM1904 is a brownish-gray micaschist with a few areas of more intense brown color.
Deformation
A poorly-defined foliation is marked by the shape preferred orientation of white mica.
Mineral composition
The mineral composition of the sample is carbonates (calcite and ankerite) 50%, quartz 20%, white mica 10% chlorite 8%, graphite 5%, rutile 3%, and ilmenite 3%. Accessory minerals (less than 2% each) tourmaline, zoisite
Timing of mineral growth with respect to deformation
Rutile in the matrix is partially replaced by ilmenite. Crystals are not very well oriented parallel to the main foliation. Some carbonate crystals are altered and may represent previous ankerite crystals. A well-preserved mm sized tourmaline with inclusions of ilmenite, graphite and calcite is observed (fig 20).
Graphite abundance and distribution
Graphite is very abundant in this sample, and is dispersed in the whole sample, although it may be concentrated in some layers parallel to the foliation. Graphite is observed as inclusions in tourmaline, carbonate, quartz, white mica, and chlorite.

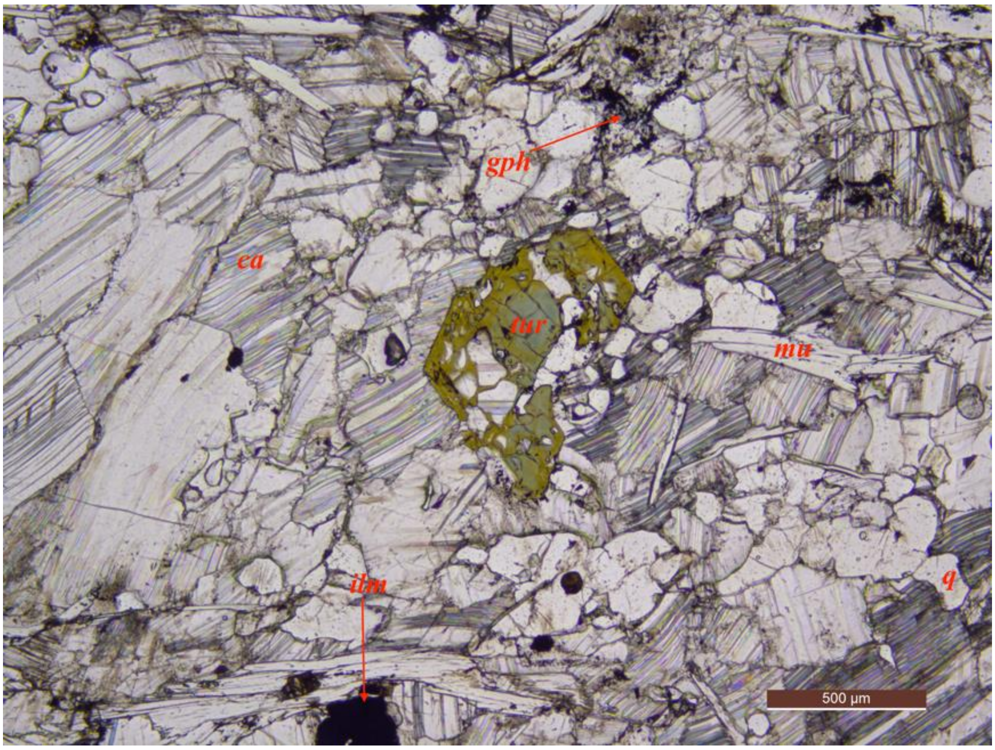

Figure 20. Calcite is covering most of this image, but in the middle there is a large zoned tourmaline displaying calcite inclusions.

GM1907: Micaschist

Macroscopic aspect
Sample GM1907 is a pale blue-green micaschist.
Deformation
The rock displays a pervasive foliation marked by quartz band, mica-rich layers, and by the shape preferred orientation of white mica and chloritoid. Rutile is aligned parallel to the main foliation.
Mineral composition
The mineral composition of the sample is white mica 40%, chlorite 22%, quartz 20 % and chloritoid 15%, sodic amphibole (5%). Accessory minerals (less than 2% each) Graphite, ilmenite, rutile and epidote
Timing of mineral growth with respect to deformation
Chloritoid contains inclusions of graphite, rutile and quartz. Chloritoid is locally zoned, with light blue cores and thin dark blue rims (fig 21). Chloritoid is partially replaced at the rim by chlorite. Elongated or lozenge-shape fine-grained aggregates consisting of chlorite and quartz are aligned parallel to the main foliation. They are interpreted as pseudomorphs after sodic amphibole.
Graphite abundance and distribution
Graphite is not so abundant in this sample, and is dispersed in the whole sample, although it may be concentrated in some layers parallel to the foliation. Graphite are observed as inclusions in quartz, chloritoid, chlorite and white mica.

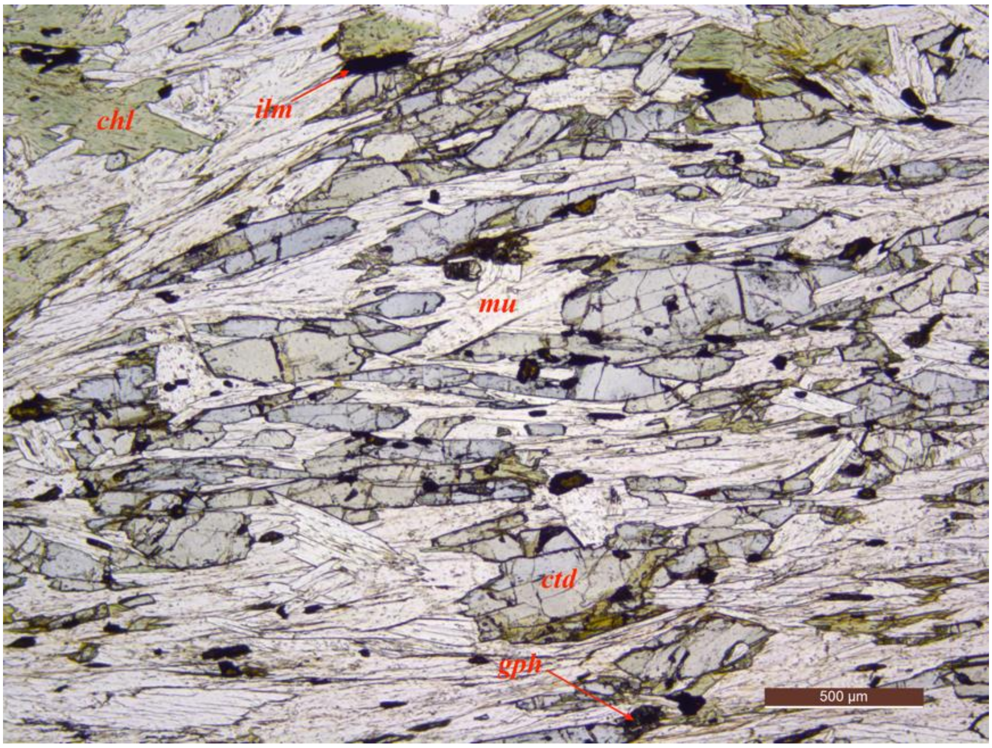

Figure 21. A main foliation is marked by chloritoid and white mica. Chloritoid is sometimes replaced by chlorite.

CH2016: Marble

Macroscopic aspect
Sample CH2016 is a grey marble with black mm sized spots dispersed on the whole sample
Deformation
A weak foliation is marked by the shape preferred orientation of white mica and by quartz lenses.
Mineral composition
The mineral composition of the sample is Carbonates 60%, white mica 10%, quartz 10%, chlorite 8%, oxides 4% and graphite 3%. Accessory minerals (less than 2% each) tourmaline and epidote.
Timing of mineral growth with respect to deformation
Big oxide crystals up to 400µm are observed with a red product covering some of the crystals rim (fig 22). The large oxide crystals are observed dispersed relatively evenly in the sample and contains inclusions of graphite and less frequently quarts. the carbonate crystals have a big variation in size from 50µm to 1mm in diameter. The carbonate crystals have inclusions of white mica, quartz, chlorite and graphite. A few 2-3mm sized quartz crystals are observed well preserved.
Graphite abundance and distribution
Graphite is abundant in this sample, and is dispersed in the whole sample, although it may be concentrated in some layers parallel to the foliation. Where the crenulations are observed the highest concentrations of graphite are observed. The graphite is concentrated on both sides of the crenulations. Graphite is also concentrated along the rims of the large ilmenite crystals. Inclusions of graphite are observed in quartz, quartz, chlorite, white mica and ilmenite.

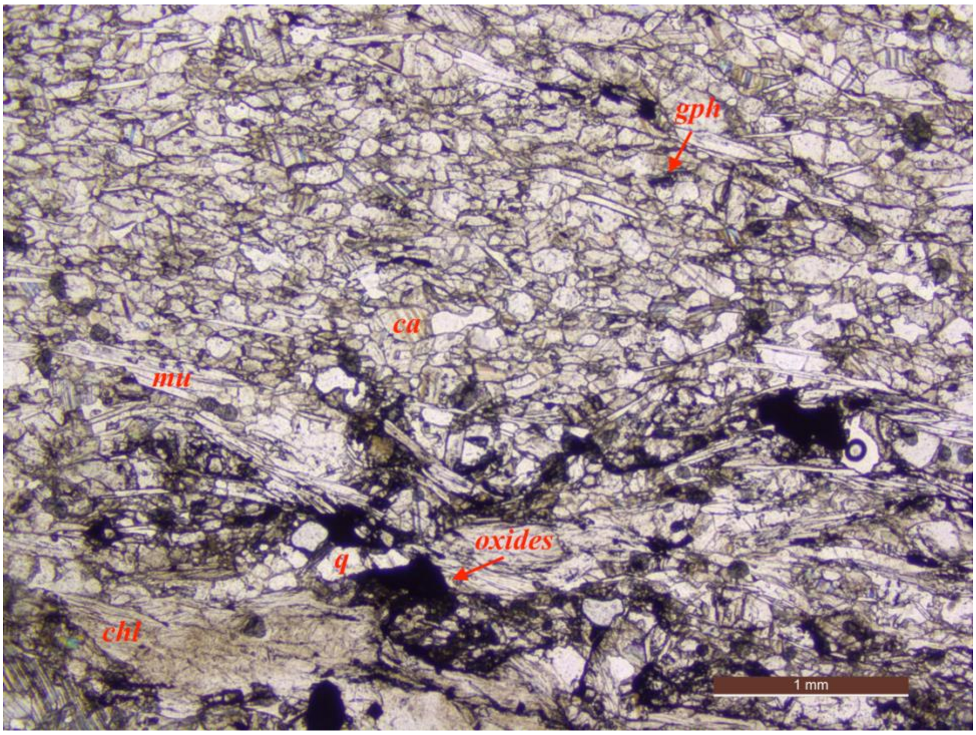

Figure 22. This sample is monotonously constituted by calcite. The image is one of the few areas in the thin section where there are some other minerals such as oxide, white mica, and graphite.

GM2004b: Calcschist

Macroscopic aspect
Sample GM2004b is a yellowish-gray calcschist.
Deformation
The rock does not display a clear foliation, but locally white mica seems to have a shape preferred orientation.
Mineral composition
The mineral composition of the sample is carbonate 60%, quartz 15%, white mica 8%, chlorite 7%, graphite 6% and albite 4%. Accessory minerals (less than 2% each) tourmaline, oxide and epidote.
Timing of mineral growth with respect to deformation
Due to the lack of a clear structure, it is very difficult to reconstruct the timing of the mineral growth in this sample. The carbonate in the sample varies in size but most crystals are in the 50µm in size. Some of them display polysynthetic twinning. The chlorite in the sample is white or yellow and are accompanying with high concentrations of graphite (fig 23).
Graphite abundance and distribution
Graphite is abundant in this sample, and is dispersed in the whole sample, although it may be concentrated in some layers randomly and not necessarily following the foliation. Graphite is observed as inclusions in carbonates, tourmaline, quartz, white mica, chlorite and ilmenite

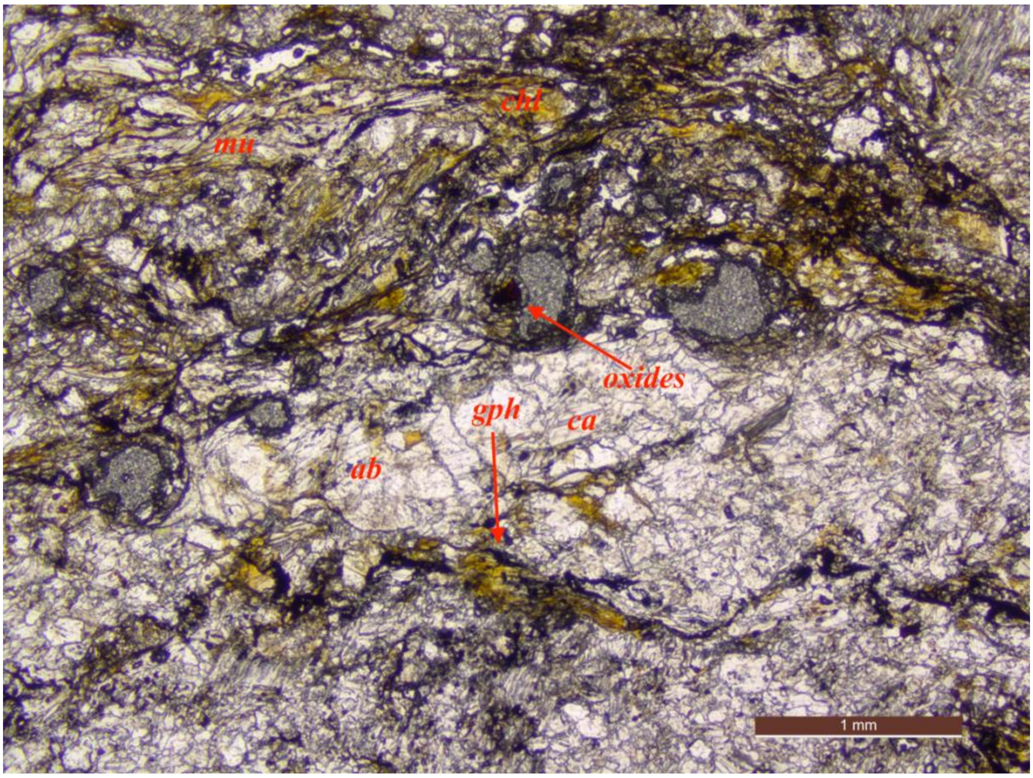

Figure 23. Yellowish chlorite is defining a weak foliation. Graphite is locally associated with chlorite.

Raccias Unit

One sample from the Raccias Unit have been analyzed

GM2029: Calcschist

Macroscopic aspect
Sample GM2029 is a grayish-brown calcschist.
Deformation
The rock displays a foliation defined by carbonate-rich domains alternated with discontinuous white mica layers and fine-grained quartz lenses. The foliation is gently folded.
Mineral composition
The mineral composition of the sample is carbonates 40%, white mica 25%, graphite 15%, chlorite 7%, oxide 5% and quartz 5%. Accessory minerals (less than 2% each) epidote, tourmaline and titanite.
Timing of mineral growth with respect to deformation
Inclusions of graphite, and quartz, are observed in white mica. (fig 24). Carbonates are very fine-grained and it is difficult to recognize single crystal. White mica crystals are strongly internally deformed and show undulose extinction.
Graphite abundance and distribution
Graphite is highly abundant in this sample, and is dispersed in the whole sample, although it may be concentrated in some layers parallel to the foliation. The graphite is mostly concentrated along the borders of the white mica, but the highest concentrations of graphite is accompanying with the crenulations. in most white mica crystals inclusions of graphite can be seen and graphite can be observed as inclusions in tourmaline, quartz and albite.

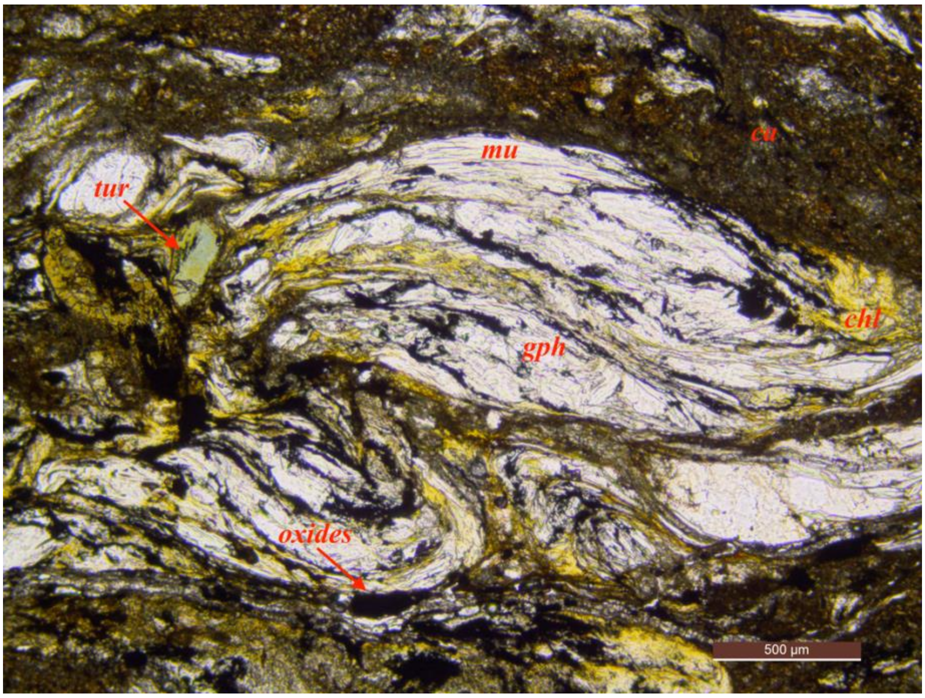

Figure 24. Highly deformed white mica flakes are associated with graphite, oxide and altered chlorite. Carbonate crystals display a rusty color.

RSCM temperatures along a cross-section through the SW Alps

Sanfront-Pinerolo Unit

Northern sector

SN1902: Graphitic micaschist
23 different graphite crystals were analyzed in this sample. Graphite yields R2 values ranging from 0.16 to 0.30, whereas R1 values are between 0.11 and 0.24. The estimated temperatures range from 510 °C to 568 °C. The maximum T registered from sample SN1902 is 501 ± 7 °C.

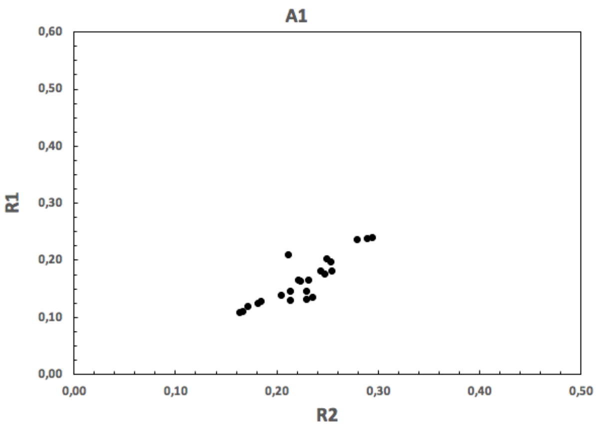

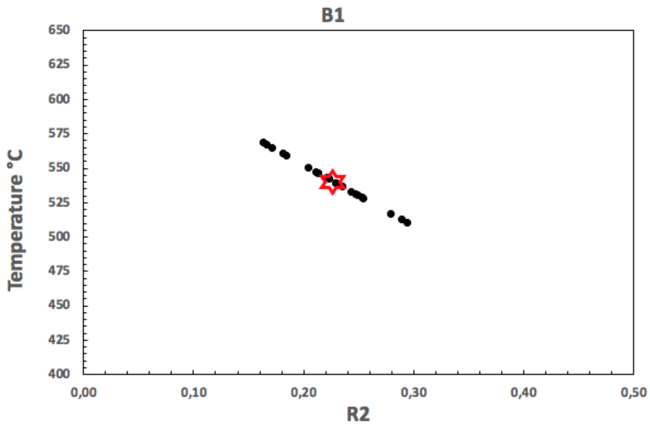

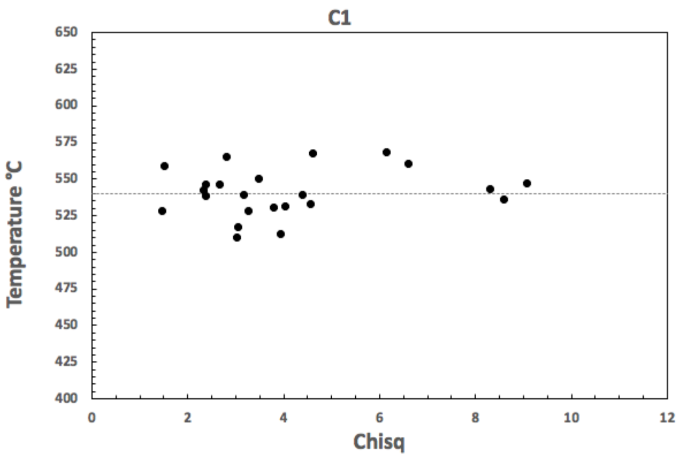

In graph A1, R1 and R2 is plotted against each other to see how reliant the data is, the data is consistent and that means the data is good. Graph B1 Temperature against R2 showing a linier pattern with no obvious outliers and the middle temperature (red star) is located in the middle of the points. Graph C is temperature against Chisq, this is not showing any obvious outlier.

CH2003: Garnet-micaschist

22 different graphite crystals were analyzed in this sample. Graphite yields R2 values ranging from 0.09 to 0.36, whereas R1 values are between 0.07 and 0.28. The estimated temperatures range from 480 °C to 599 °C. The maximum T registered from sample CH2003 is 531 ± 9 °C.

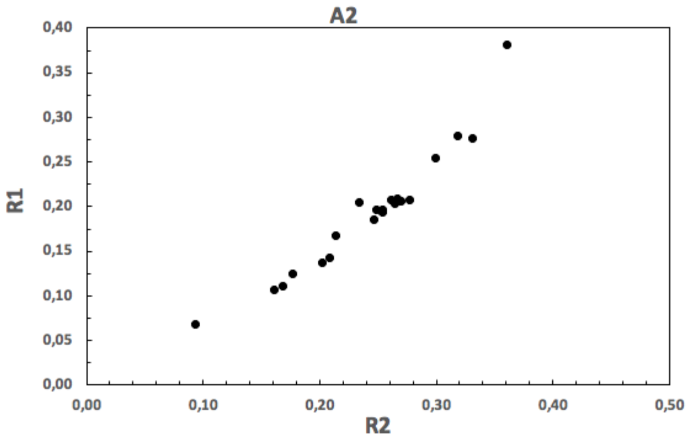

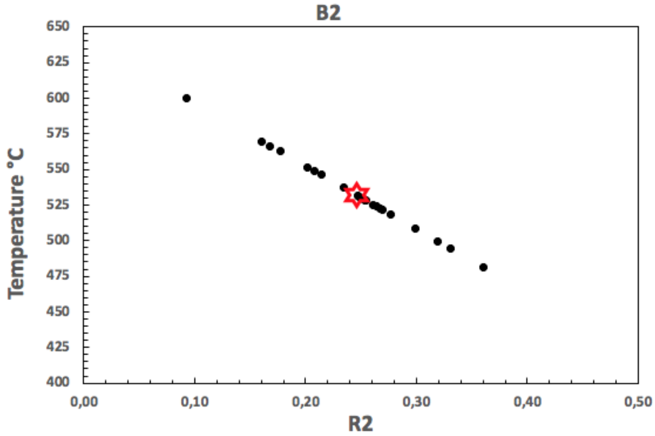

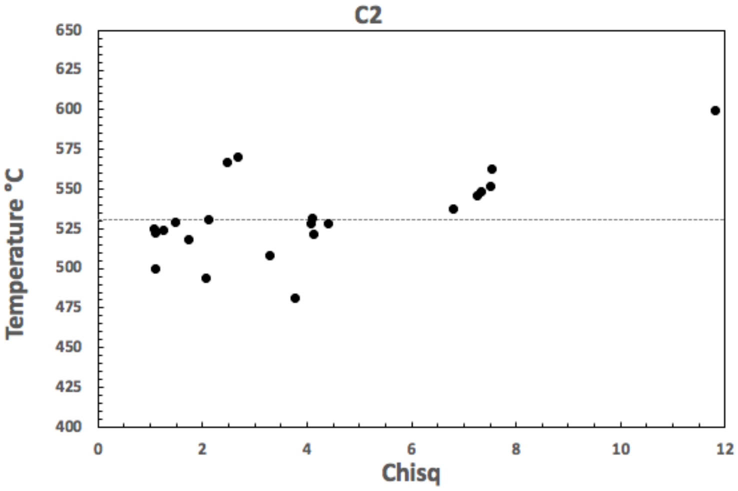

Graph A2 is showing two outliers in each end of the graph but over all the data is consistent. Graph B just showing one outlier compare to two in graph A2. The outlier data point has a higher temperature, the rest of the data is consistent. The outlier can be caused by the Raman laser cooking the graphite due to long exposure to the laser or it could be caused by the polishing proses. In the case of it being the polishing process, the aiming of the laser is to shallow in the performance of the Raman. In graph C2 there is still the same outlier to be seen but as previous graphs overall the data is consistent.

GM1404b: Graphitic micaschist

16 different graphite crystals were analyzed in this sample. Graphite yields R2 values ranging from 0.10 to 0.29, whereas R1 values are between 0.05 and 0.23. The estimated temperatures range from 510 °C to 597 °C. The maximum T registered from sample GM1404b is 551 ± 12 °C.

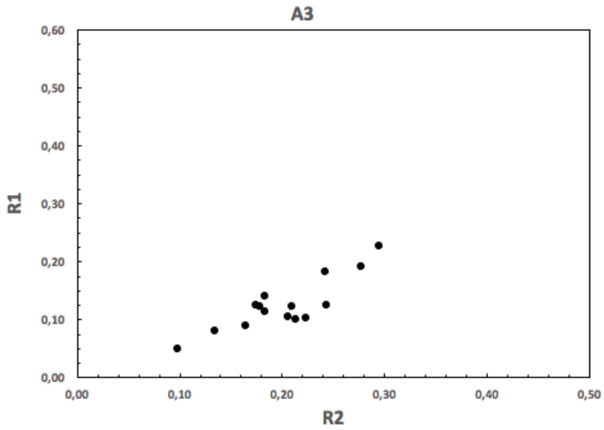

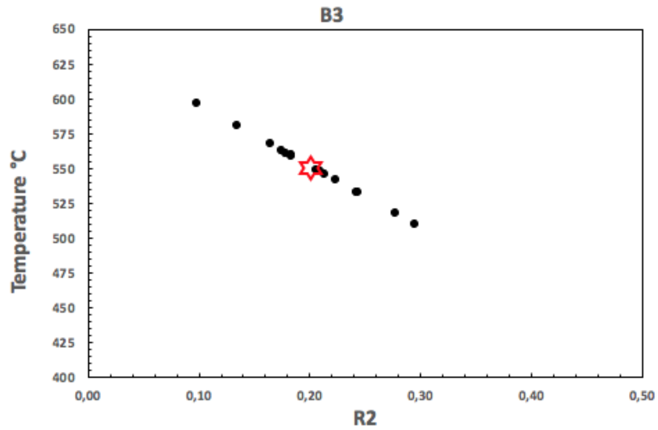

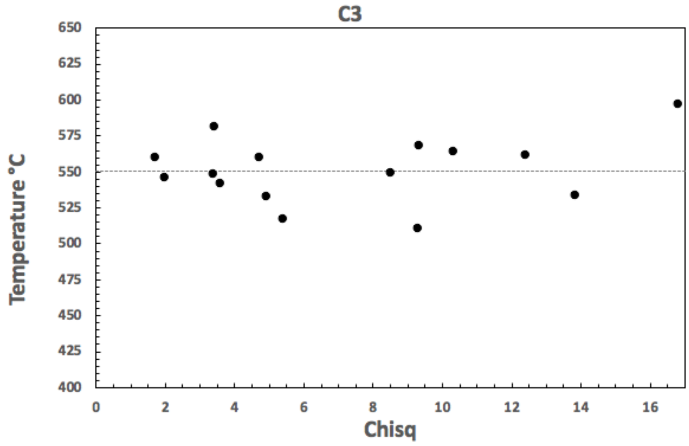

In graph A3 both R2 and R1 have low values with good consistently in the data points and no obvious outliers. Graph B3 is showing the same good pattern of data points with no obvious outliers, but this sample only have 16 graphite crystals analyzed so this can have an influence on the good consistently of the data. In graph C3 there is consistency in the temperatures, but it looks like there is two groups of higher and lower Chisq values with one data point that is close to be an outlier.

GM1405a: Graphite micaschist

21 different graphite crystals were analyzed in this sample. Graphite yields R2 values ranging from 0.14 to 0.40, whereas R1 values are between 0.1 and 0.44. The estimated temperatures range from 465 °C to 579 °C. The maximum T registered from sample GM1405a is 538 ± 10 °C.

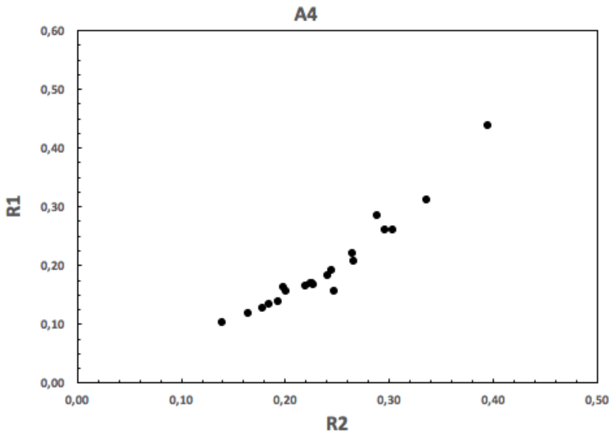

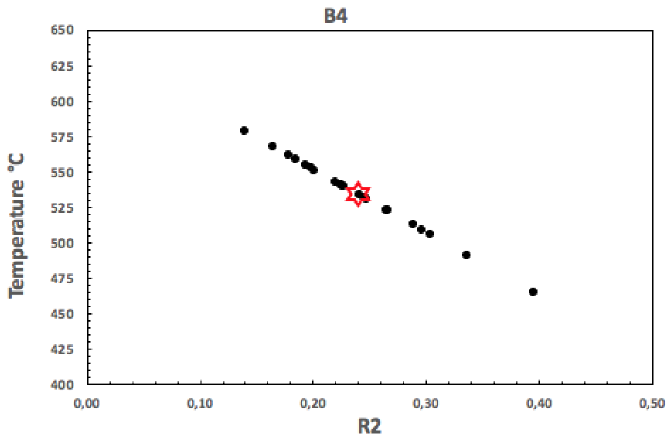

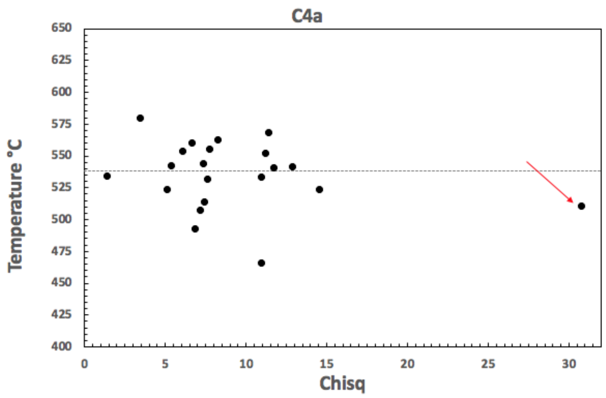

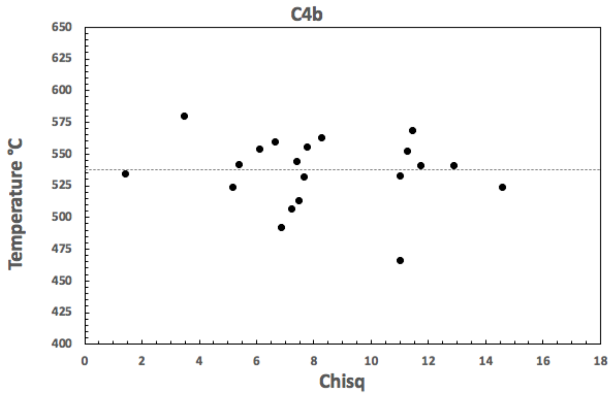

In graph A4 there is clear that there is one outlier but overall the data is consistent. In graph B4 the same data point that was outlining in A4 can be seen outlining in this graph as well. Subtracting the outlining point the data is in good consistency. In graph C4 the data points are gathered in two groups, one at around Chisq 6 and the other group around Chisq 12, but there is one outlier in the Chisq data with a value of over 30 Chisq. Apart from that data point it is consistent.

GM1419b: Graphitic micaschist

22 different graphite crystals were analyzed in this sample. Graphite yields R2 values ranging from 0.14 to 0.35, whereas R1 values are between 0.09 and 0.33. The estimated temperatures range from 484 °C to 578 °C. The maximum T registered from sample GM1419b is 539 ± 9 °C.

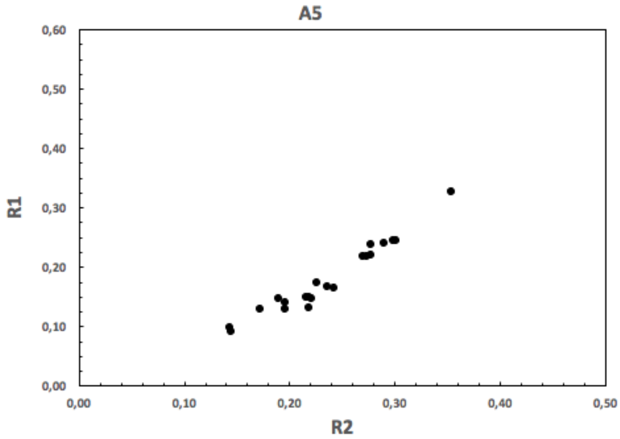

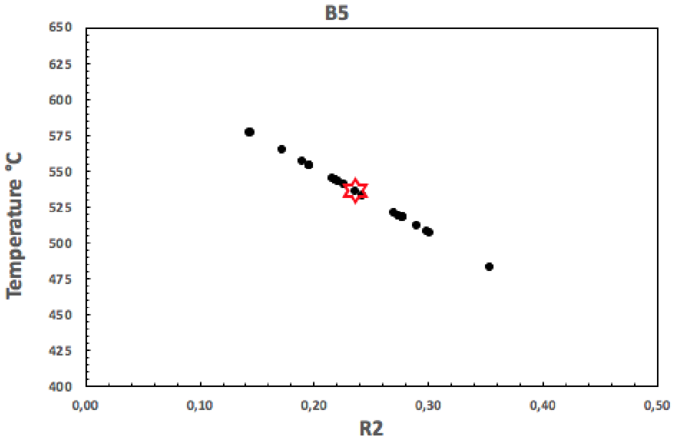

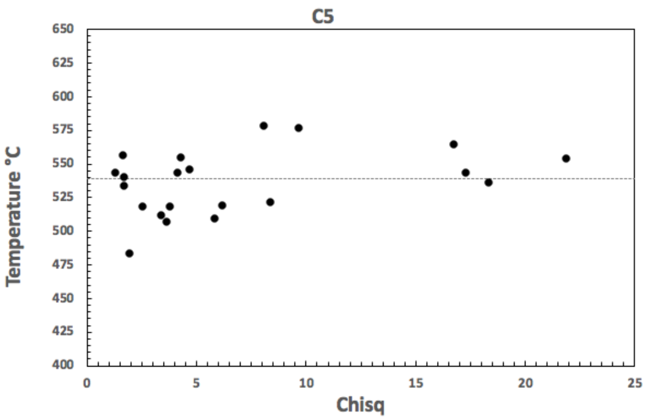

In graph A5 the data points are consistent but there is one data point that are a bit of an outlier. Graph B5 is also consistent in the data points but have the same outlier as in graph A5 but outer then that data points the data is consistent. In graph C5 the data is consistent in the temperature data but some spreading in the Chisq values and it is divided in to two groups. Most of the data points are concentrated in the low Chisq values and there is 4 points gathered in the higher Chisq values.

GM1406a: Graphitic micaschist

24 different graphite crystals were analyzed in this sample. Graphite yields R2 values ranging from 0.11 to 0.45, whereas R1 values are between 0.04 and 0.45. The estimated temperatures range from 439 °C to 591 °C. The maximum T registered from sample GM1406a is 551 ± 9 °C.

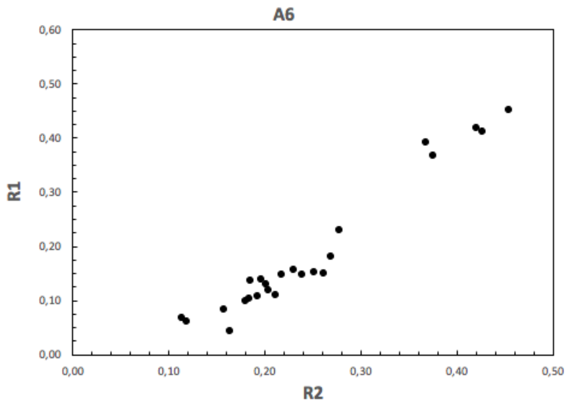

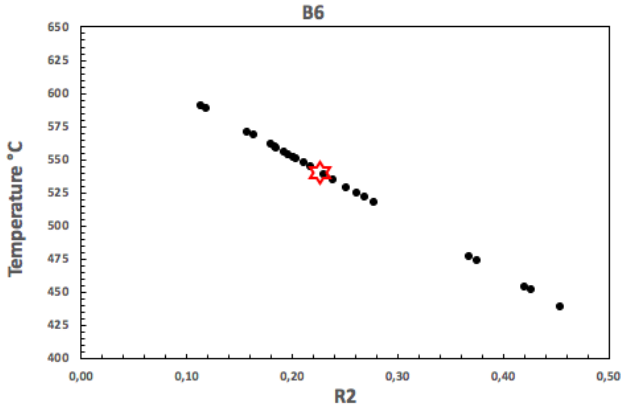

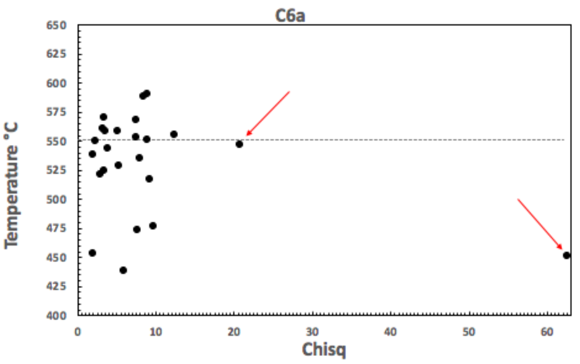

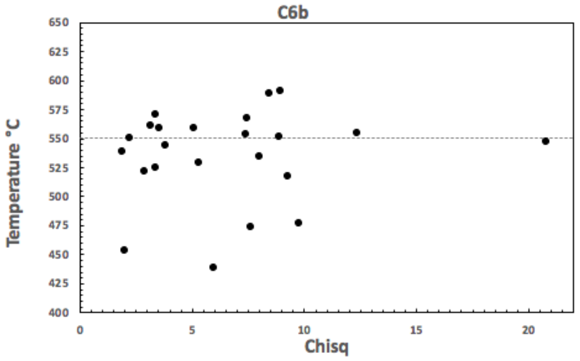

In graph A6 there is consistency of the data points but there are two areas where all the points are gathered. Most of the data points are gathered at the low R2 and R1 values but there are five points gathered in the slightly higher values. It could be a performance error by cocking the graphite with the laser, but it is most lightly not do to the quantities of data points in the higher R2 and R1 region. In Graph C6a there is some clear outliers marked with arrows, but apart from that the data is consistent. This consistency can easier be seen in the graph C6b where the biggest outlier is excluded from the data.

GM1908: Graphitic micaschist

21 different graphite crystals were analyzed in this sample. Graphite yields R2 values ranging from 0.15 to 0.45, whereas R1 values are between 0.10 and 0.42. The estimated temperatures range from 439 °C to 576 °C. The maximum T registered from sample GM1908 is 531 ± 11 °C.

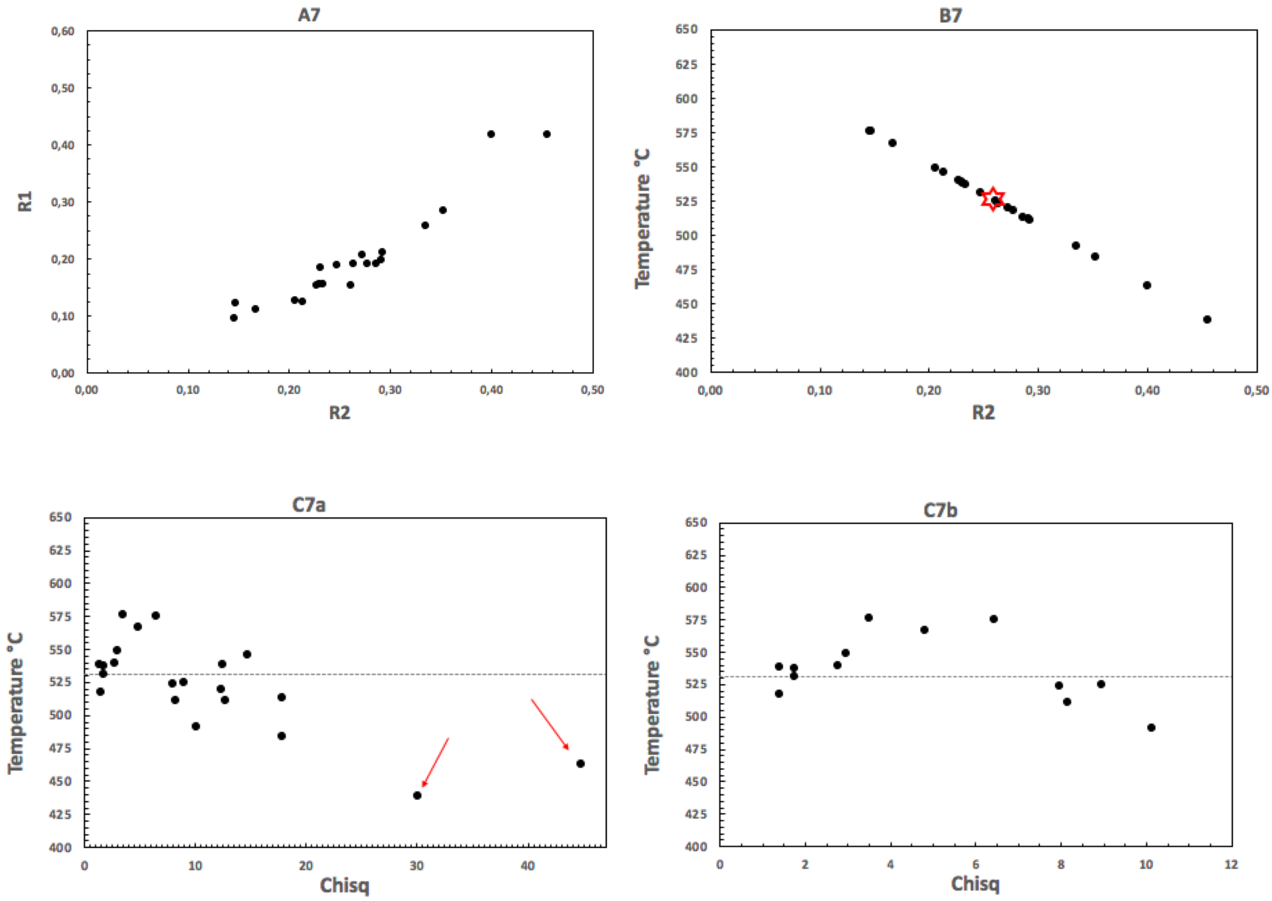

In graph A7 the data points contain two outliers but apart from those outliers the data is consistent. In graph B7 the same data points can be seen as outliers and the rest of the data is consistent. In graph C7a the same data points are outliers and in the graph these outliers are really standing out. In graph C7b the outliers are excluded and its clear that these data points are consistent. Comparing the consistent data points in the graphs C7a and C7b, in C7a its looks like the data points are divided in to two groups, but in graph C7b its clear that the data points are more like one unit.

CH1902: Graphitic micaschist

22 different graphite crystals were analyzed in this sample. Graphite yields R2 values ranging from 0.03 to 0.49, whereas R1 values are between 0.02 and 0.63. The estimated temperatures range from 421 °C to 628 °C. The maximum T registered from sample CH1902 is 568 ± 17 °C.

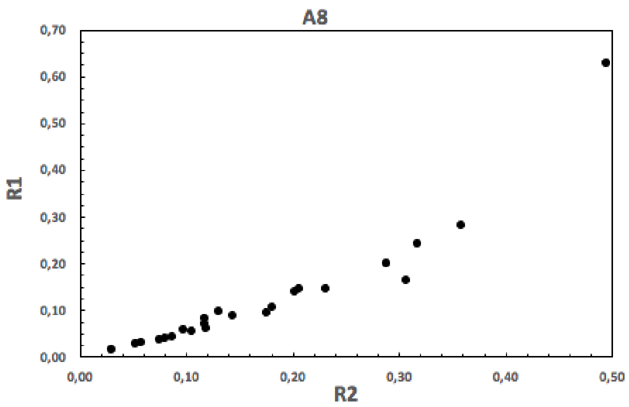

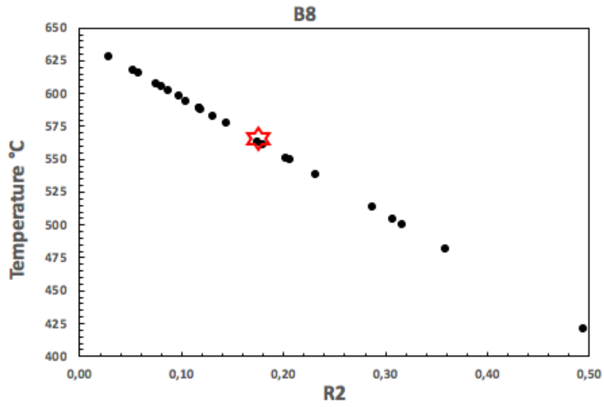

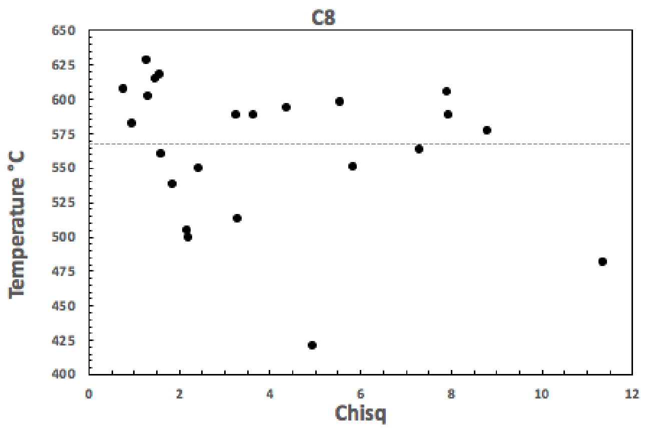

Graph A8 is showing good consistency in the data points with one outlier as an exception. This outlying data point is showing high values in both R1 and R2. Graph B8 is also showing this outlier and it is clear that this data point has much lower temperature then the others. in graph C8 it looks like it is two outliers but if one look at the temperatures of these points its clear the there is only one outlier.

Southern sector

PO2081: Graphitic micaschist

23 different graphite crystals were analyzed in this sample. Graphite yields R2 values ranging from 0.2 to 0.27, whereas R1 values are between 0.12 and 0.25. The estimated temperatures range from 512 °C to 553 °C. The maximum T registered from sample PO2081 is 532 ± 5 °C.

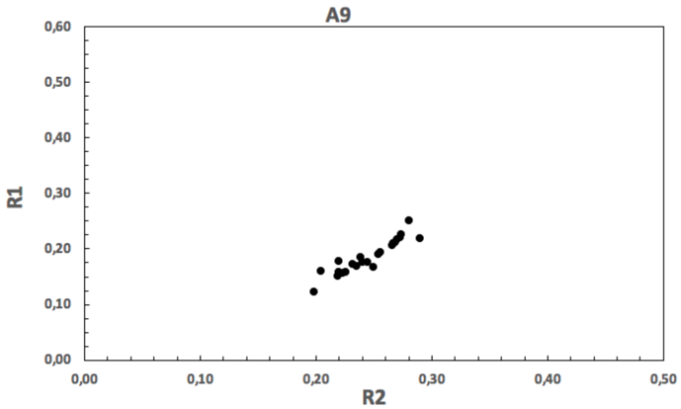

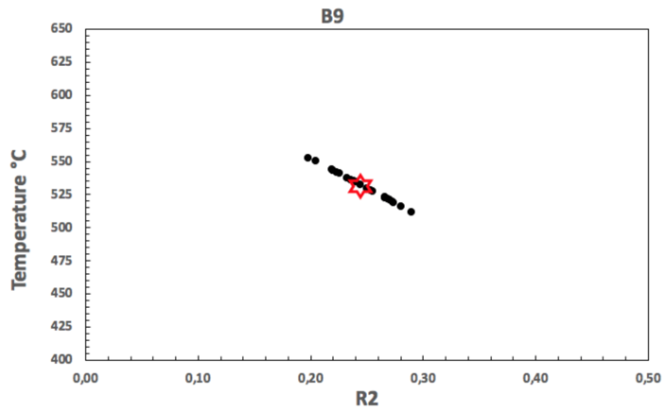

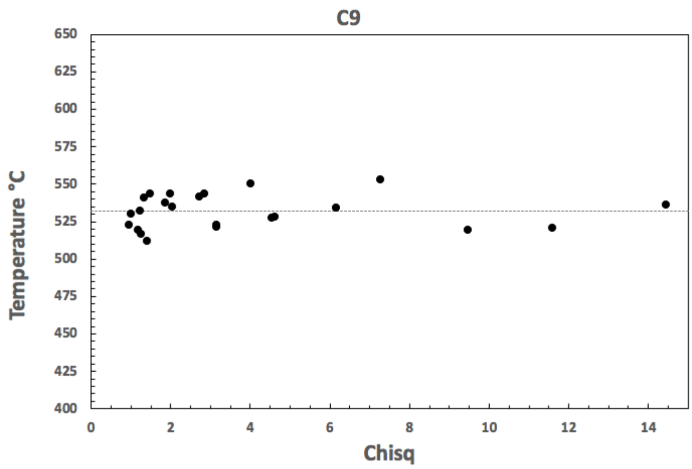

Graph A9 is showing data points with really good consistency and this good consistency of the data points is seen in graph B9 as well. In graph C9 the consistency in the temperature data is really good but in Chisq it is not as pronounced, it is still good consistency. One could argue that there are some outliers, but this is mostly because the data points is so consistent.

Chasteiran Unit

CH1907-2: Garnet chloritoid micaschist

21 different graphite crystals were analyzed in this sample. Graphite yields R2 values ranging from 0.2 to 0.33, whereas R1 values are between 0.13 and 0.33. The estimated temperatures range from 493 °C to 554 °C. The maximum T registered from sample CH1907-2 is 532 ± 6 °C.

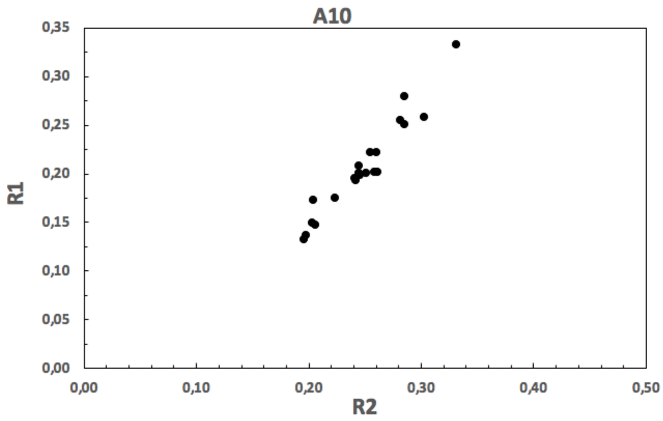

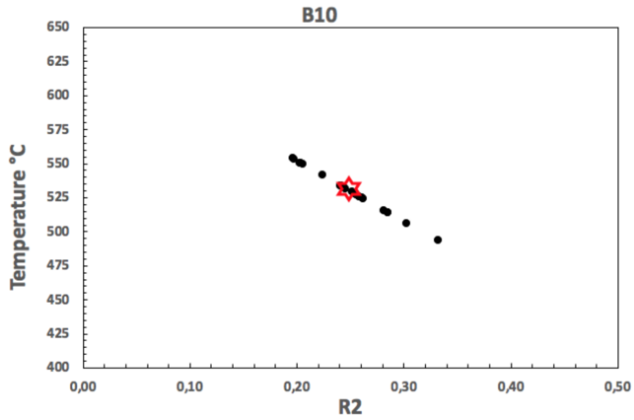

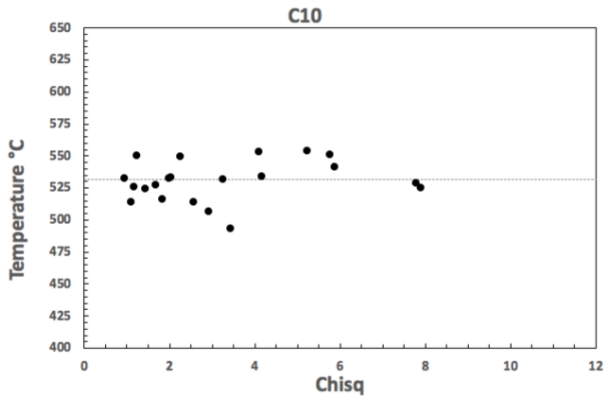

Graph A10 is showing data points with really good consistency and this good consistency of the data points is seen in graph B10 as well. In graph C10 there is consistency in both temperature data and Chisq data. The highest Chisq data point is really low indication on good data.

GM2010: Garnet micaschist

23 different graphite crystals were analyzed in this sample. Graphite yields R2 values ranging from 0.15 to 0.45, whereas R1 values are between 0.05 and 0.58. The estimated temperatures range from 439 °C to 574 °C. The maximum T registered from sample GM2010 is 526 ± 12 °C.

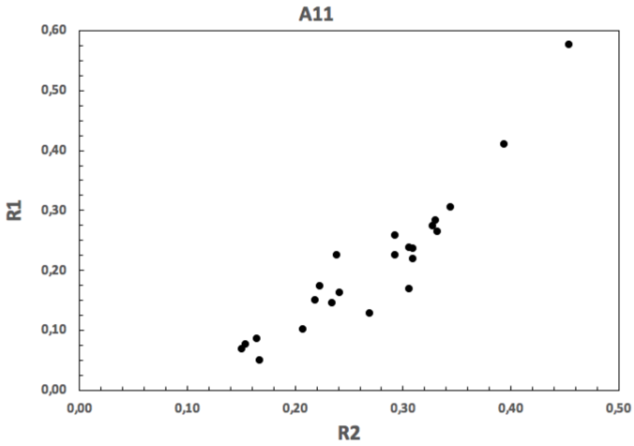

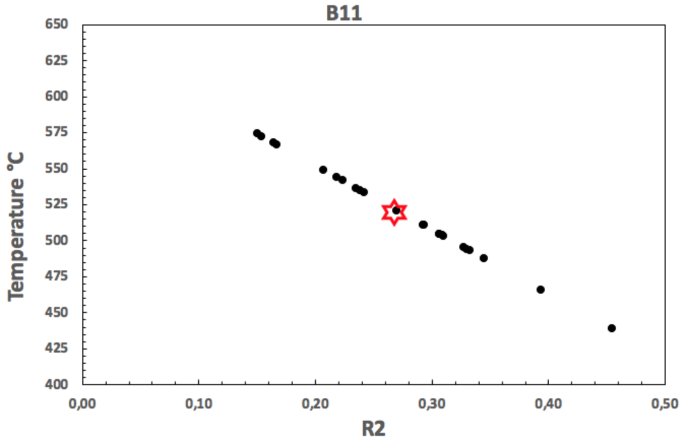

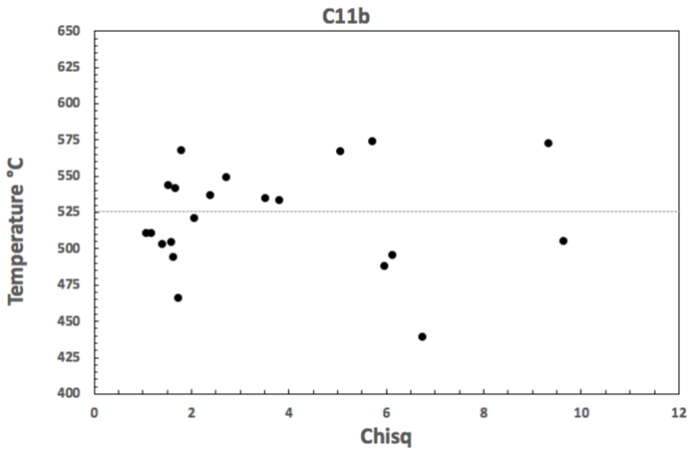

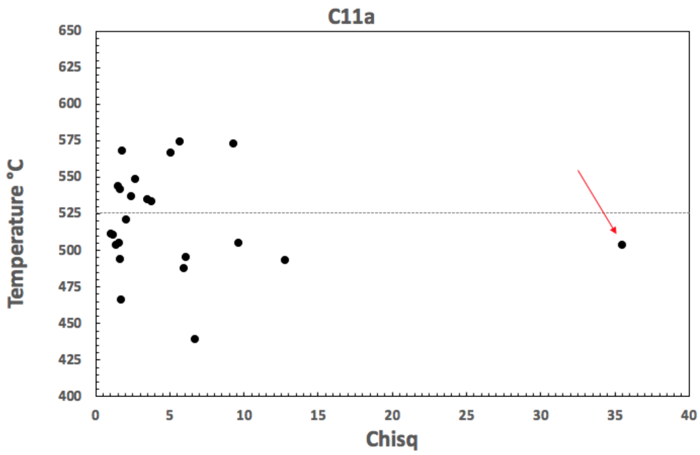

In graph A11 the data points are on good consistency but with one obvious outlier. The same pattern in the data points with the same data points as an outlier can be seen in graph B11. In graph C11a there is a different data point as an outlier, but this point is clearly an outlier by looking at the Chisq data. In graph C11b the outlier is excluded, and the data looks to have good consistency.

Serre Unit

GM1904: Calcschist

15 different graphite crystals were analyzed in this sample. Graphite yields R2 values ranging from 0.32 to 0.55, whereas R1 values are between 0.36 and 0.55. The estimated temperatures range from 396 °C to 501 °C. The maximum T registered from sample GM1904 is 480 ± 8 °C.

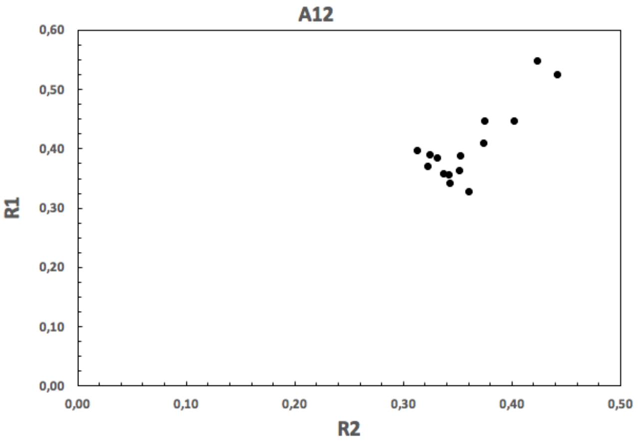

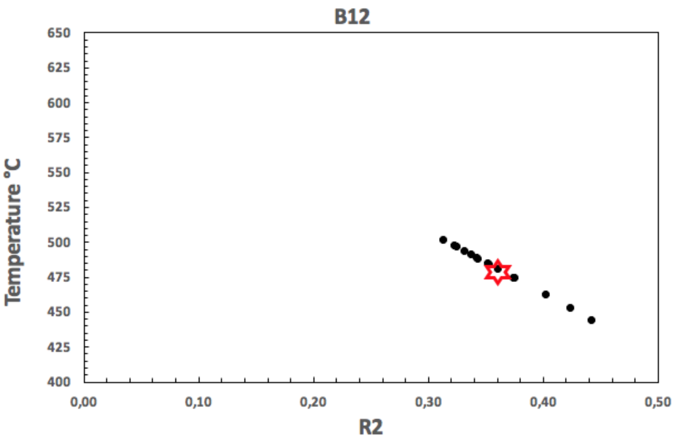

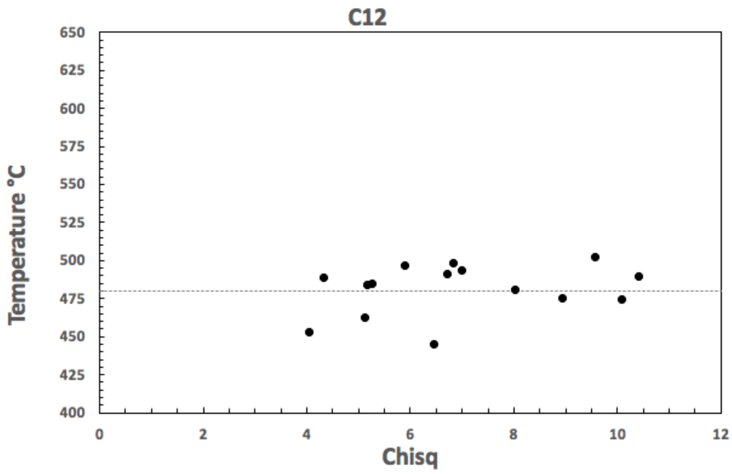

Graph A12 is showing good consistency of the data points with no outliers. Graph B12 is also showing really good consistency of the data points and no outliers. In Graph C12 the consistency of the data points is still there both in the Chisq and the Temperature. The good consistency of the data can be a result of the low amount of data curves used.

GM1907: Garnet micaschist

22 different graphite crystals were analyzed in this sample. Graphite yields R2 values ranging from 0.12 to 0.46, whereas R1 values are between 0.06 and 0.51. The estimated temperatures range from 437 °C to 588 °C. The maximum T registered from sample GM1907 is 500 ± 20 °C.

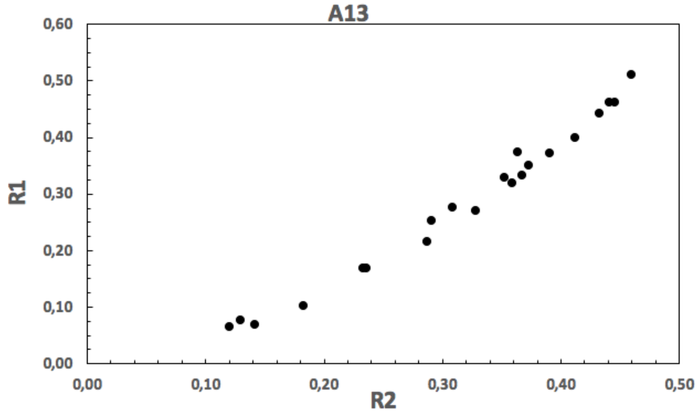

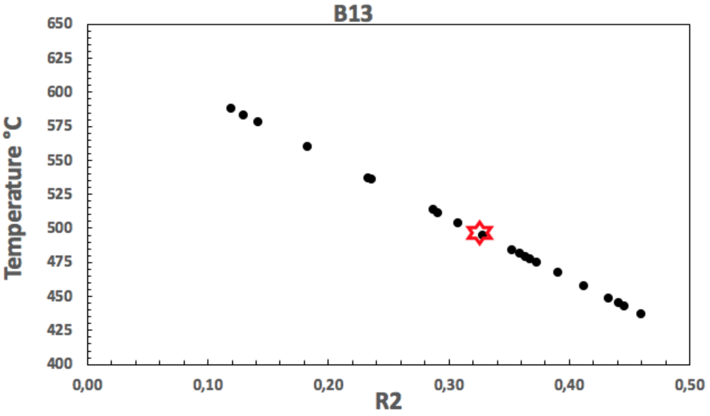

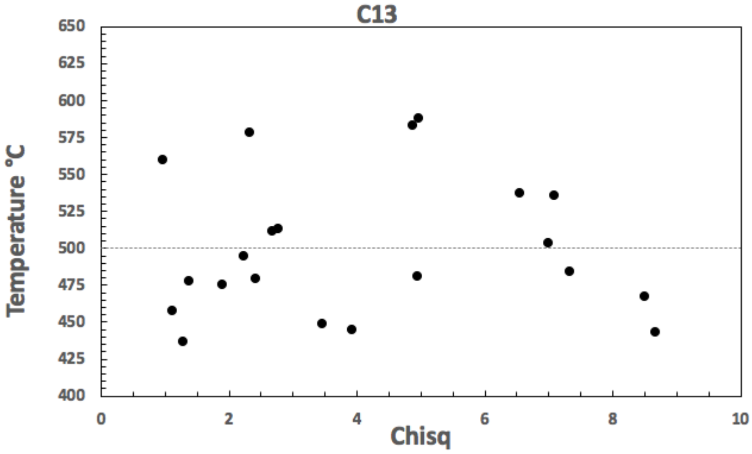

In graph A13 the data points show a pattern of good consistency with no obvious outliers. Graph B13 also show good consistency in the data points, but it is more pronounced in this graph that data points are more centered in the high R2 values. In graph C13 the consistency of the data points continues, and the temperature data is dispersed from the highest temperature to the lowest temperature close to evenly.

CH2016: Marble

21 different graphite crystals were analyzed in this sample. Graphite yields R2 values ranging from 0.12 to 0.39, whereas R1 values are between 0.1 and 0.37. The estimated temperatures range from 467 °C to 587 °C. The maximum T registered from sample CH2016 is 513 ± 7 °C.

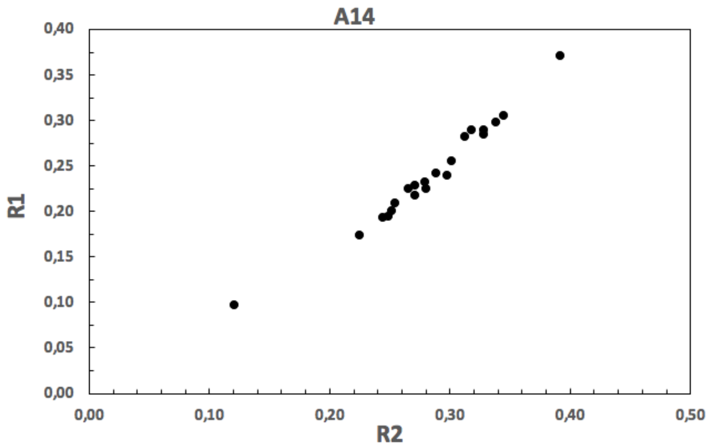

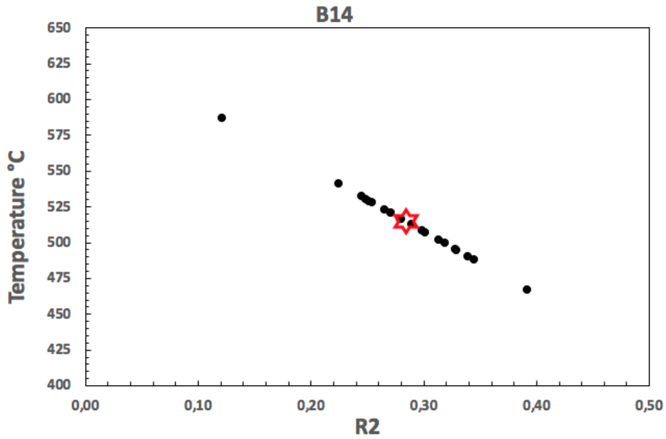

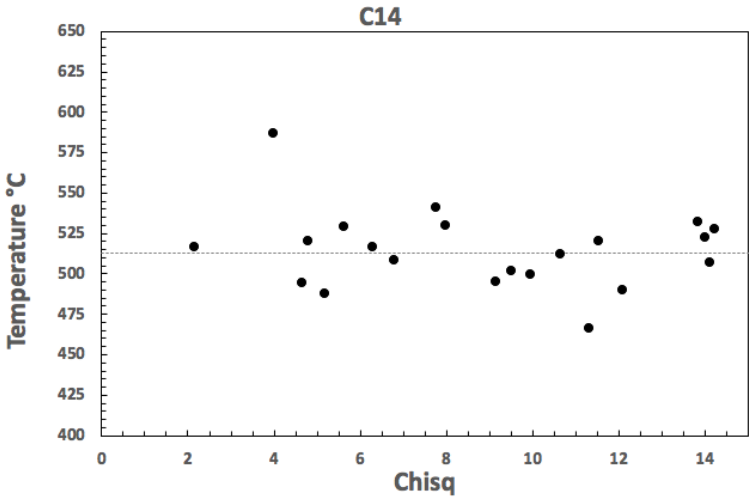

In graph A14 the data points are on good consistency but with one obvious outlier and one that is on the brink of being an outlier. The same pattern in the data points can be seen in graph B14 but here its more indicative that there is one outlier in the data points and not two. In graph C14 the data points are in good consistency and there is no obvious outlier.

GM2004b: Calcschist

21 different graphite crystals were analyzed in this sample. Graphite yields R2 values ranging from 0.28 to 0.45, whereas R1 values are between 0.21 and 0.57. The estimated temperatures range from 443 °C to 519 °C. The maximum T registered from sample GM2004b is 492 ± 6 °C.

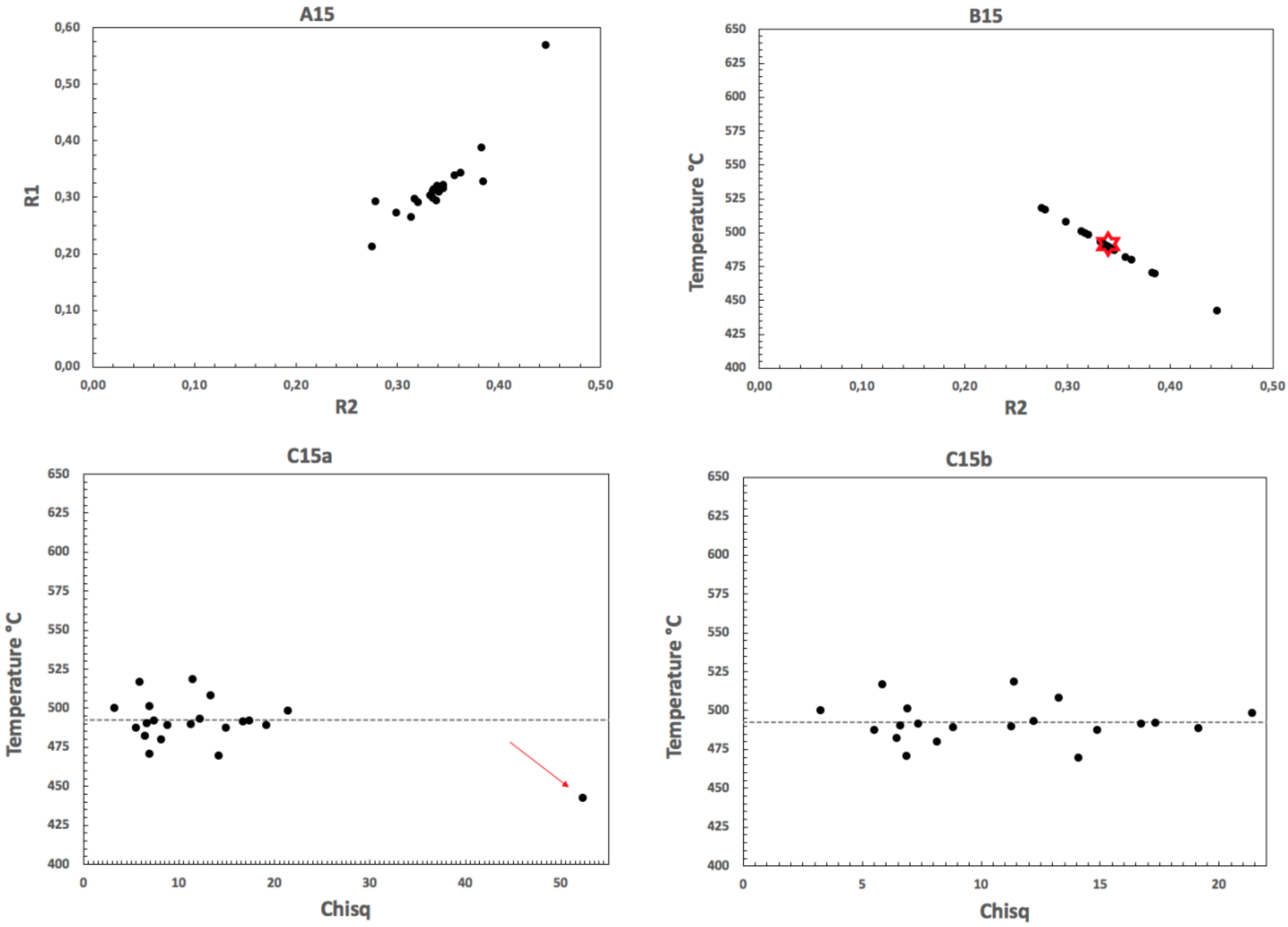

In graph A15 the data points are in good consistency but with one obvious outlier. The same pattern in the data points with the same data points as an outlier can be seen in graph B15. The outlier data point in graph B15 is not as pronounced as in graph A15. In graph C15a the same outlining data point is seen in the far-right end of the graph clearly showing that it is an outlier. Apart from that data point the data is consistent as seen in graph C15b where the outlier has been excluded.

Raccias Unit

GM2029: Calcschist

21 different graphite crystals were analyzed in this sample. Graphite yields R2 values ranging from 0.24 to 0.39, whereas R1 values are between 0.17 and 0.37. The estimated temperatures range from 467 °C to 535 °C. The maximum T registered from sample GM2029 is 501 ± 7 °C.

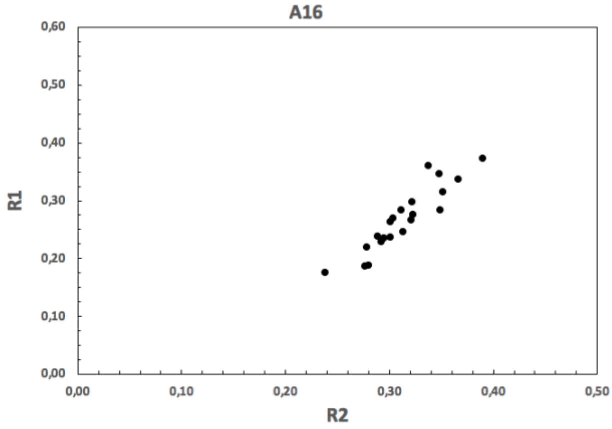

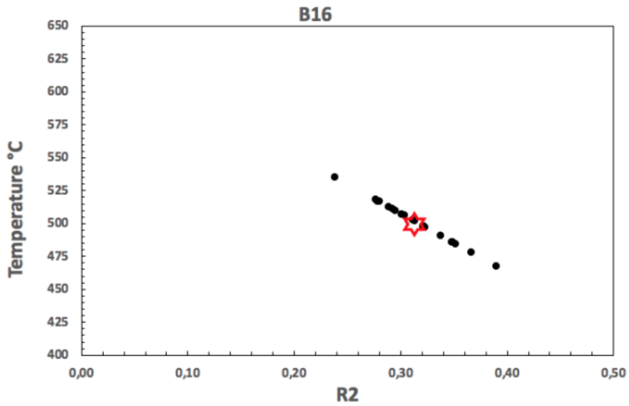

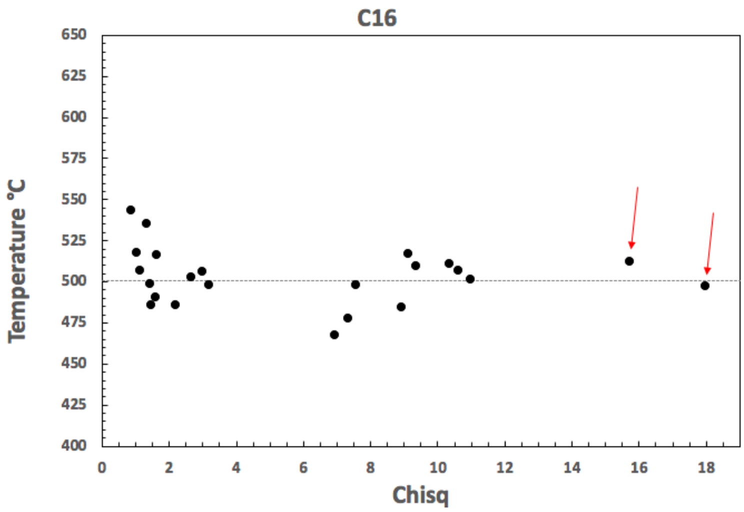

In graph A16 the consistency of the data points is close to perfect. This consistency is continuing in graph B16 as well with almost a black line buildup of the data points. In graph C16 the consistency is not as pronounced as in A16 and B16. It is instead separated in to two groups of data points where the Chisq is dividing them. In graph C16 there is two outliers also marked with red arrows.

RSCM temperatures: a summary

Graph 17-18 is a summary of the RSCM investigations. Within the Dora-Maira Massif, the units display a gradual decrease in temperature from bottom to top. The Sanfront-Pinerolo Unit recorded the highest T, in the range 531-568°C, the Chasteiran Unit recorded the highest T, in the range 526-532°C and the Serre Unit recorded the highest T, in the range 480-513°C.
One sample has been analyzed in the oceanic eclogite-facies Raccias Unit. This unit recorded a slightly higher temperature than the Serre Unit with highest T of 501°C (table 1).

Graph 17:

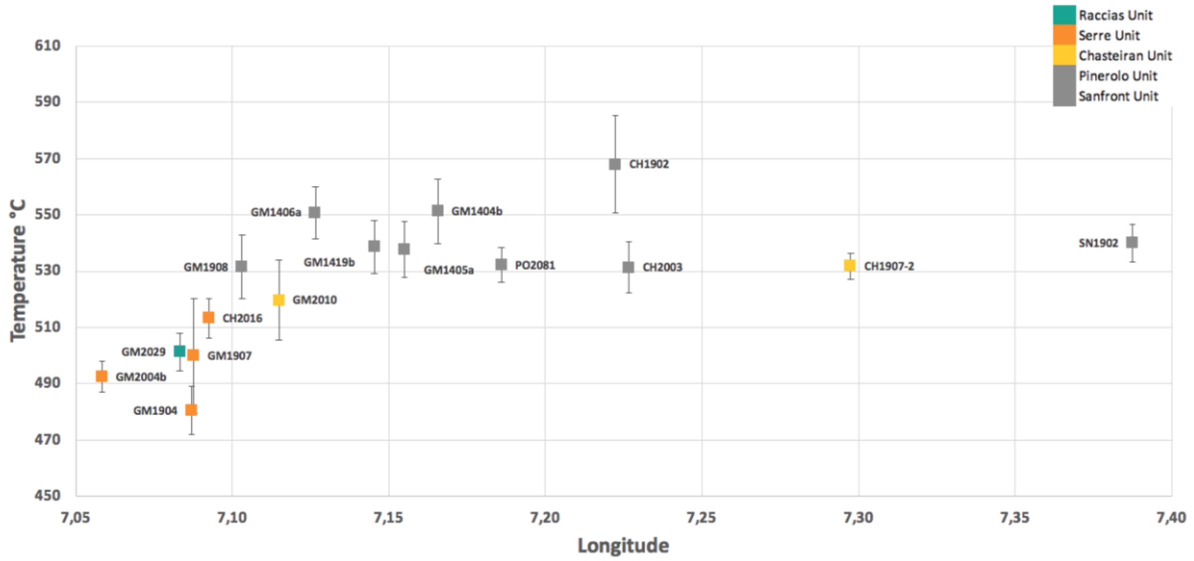

In graph 17 all the samples are gathered and plotted with temperature against longitude. Every sample is plotted with the average temperature and the error margin is applied on every sample. The legend in the up-right corner is color-coded by unit and by looking at the graph one can see that the Chasteiran Unit is surfacing in the low longitude and the high longitude. Most of the other samples are proximal to the other samples from the same unit. looking at the temperature unit wise the temperatures are consistent in the units but comparing unit buy unit it is big difference.

Graph 18:

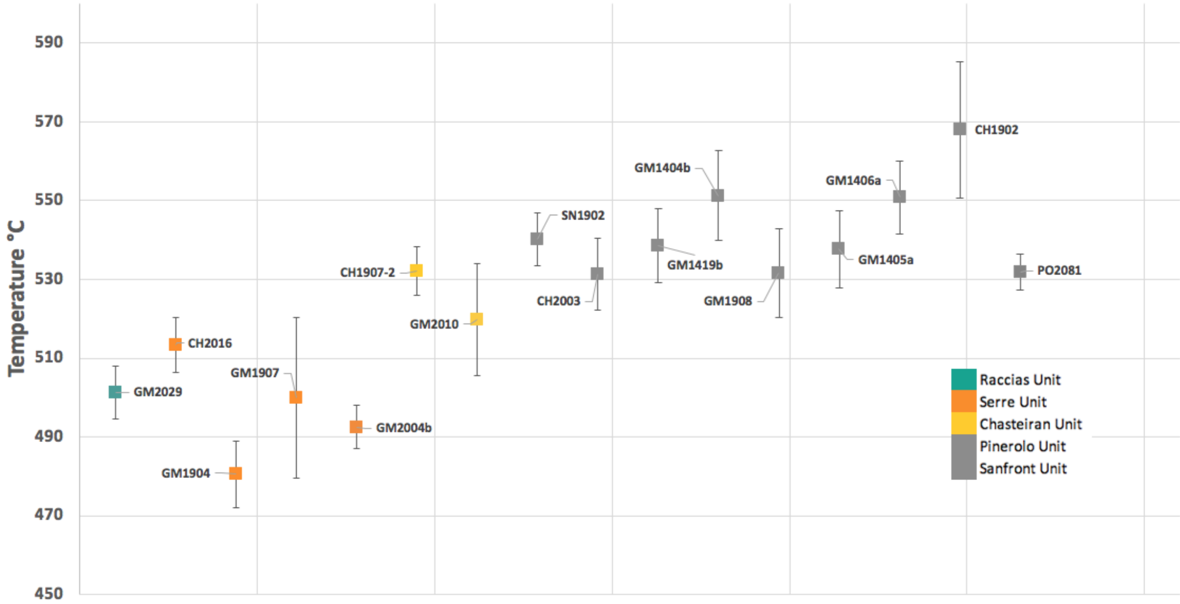

In graph 18 the samples x-axis is dividend according to their unit but within the unit also by longitude and on the y-axis the temperature. Every sample is applied with their error margin and the legend is color-coded by the unit. Raccias Unit looks to be in the same temperature or even higher then Serre Unit, but this could be an error due to there is just one sample from Raccias and therefore this could be a sample in the upper temperature in that unit. over all the unit temperatures is in the order of, Raccia Unit or Serre Unit in the low temperature and then Chasterian Unit → Pinerolo Unit → Sanfront Unit.

Analytical difficulties encountered during the investigations

Sample GM1904 was difficult to analyze. This is due to the small modal amount of graphite and its small grain size, resulting in a weak graphite signal and high background noise. In sample SN1902, GM1904a and GM1908 diamonds were detected instead of graphite. After careful investigations, we attributed this to the fact that these three thin sections have been done and polished using diamond paste (Aoya et al 2010).

Table 1:

Sample	Lithology	Unit	GPS Lat Long coordinates	Mineral assemblage: Main minerals	Mineral assemblage: Accessory minerals (less than 2% each)	n	R2	T (°C)	SD	Confidence
SN1902	graphitic micaschist	Pinerolo Unit	44°59'34.63"N 7°23'15.11"E	gph 40%, q 25%, mu 13%, chl 7%	Oxides	23	0.16-0.30	540	16	7
CH2003	g-ctd micaschist	Pinerolo Unit	44°57'30.54"N 7°13'36.29"E	q 30 %, chl 25%, mu 20 %, g 10%, ilm 5%, gph 5%, sph 5%	ep, ru, ab, bi, ctd, py	22	0.09-036	531	21	9
GM1404b	micaschist	Pinerolo Unit	44°57'3.02"N 7°9'56.45"E	q 55%, ab 25%, mu 8%, chl 7%	gph, ilm, sph, g	16	0.1-0.29	551	23	12
GM1405a	micaschist	Pinerolo Unit	44°56'25.52"N 7°9'18.17"E	q 42%, ab 20%, chl 15%, mu 5 %, gph 5%, g 3%	ilm, bi	21	0.14-0.40	538	22	10
GM1419b	graphitic micaschist	Pinerolo Unit	44°57'20.37"N 7°8'43.42"E	q 38%, chl 20%, mu 15%, ab 5%, bi 5%, gph 4%, ilm3 %	tur, g, ep	22	0.14-0.35	539	21	9
GM1406a	graphitic micaschist	Pinerolo Unit	44°56'16.11"N 7°7'35.59"E	ab 30%, mu 20%, chl 17%, q 15%, g 10%, ilm 6%	gph, ep, ca, bi, sph, tur	24	0.11-0.45	551	21	9
GM1908	graphitic micaschist	Pinerolo Unit	44°56'28.54"N 7° 6'11.40"E	q 28%, chl 20%, mu 15%, ab 5%, g 5%, ilm 5%, gph 4% bi 4%	tur, ep, sph	21	0.15-0.45	531	25	11
CH1902	graphitic micaschist	Pinerolo Unit	44°54'4.51"N 7°13'20.77"E	chl 35%, mu 17%, ab 16%, q 13%, g 9%, ilm 4% gph 3%	ru, bi, sph, ctd, ep	22	0.03-0.49	568	17	17
PO2081	graphitic micaschist	Sanfront Unit	44°38'39.45"N 7°17'51.07"E	ab 35%, q 25%, gph 15%, ilm 10%, chl 5%, mu 3%	ru	23	0.20-0.27	532	11	5
CH1907-2*	g-ctd micaschist	Chasterian Unit	44°55'42.43"N 7°11'9.39"E	mu 35%, q 30%, chl 16%, ctd 6%, ab 4%, ilm 4%	tur, gph, g, sph, ep	21	0.20-0.33	532	14	6
GM2010	g-gl micaschist	Chasterian Unit	44°55'33.46"N 7° 6'53.74"E	q 30%, mu 25%, chl 20%, bi 10%, ab 5%, g 5%, sodiac amphebole 5%	ru, gph, ilm, ep	23	0.15-0.45	526	28	12
GM1904	calcschist	Serre Unit	44°58'20.56"N 7° 5'13.12"E	ca 50%, q 20%, mu 10% chl 8%, gph 5%, rutile 3%, ilm 3%	tur, zo	15	0.32-0.55	480	17	8
GM1907*	micaschist	Serre Unit	44°58'19.37"N 7° 5'15.95"E	mu 40%, chl 22%, q 20 %, ctd 15%, sodiac amphebole 5%	gph, ilm, ru, ep	22	0.12-0.46	500	48	20
CH2016	marble	Serre Unit	44°59'6.27"N 7° 5'33.09"E	ca 60%, mu 10%, q 10%, chl 8%, oxides 4%, gph 3%	tur, ep	21	0.12-0.39	513	16	7
GM2004b	calcschist	Serre Unit	44°55'16.88"N 7° 3'30.24"E	ca 60%, q 15%, mu 8%, chl 7%, gph 6%, ab 4%	tur, oxides, ep	21	0.28-0.45	492	13	6
GM2029	calcschist	Raccias Unit	44°58'27.61"N 7°4'59.71"E	ca 40%, mu 25%, gph 15%, chl 7%, oxides 5%, q 5%	ep, tur, sph	21	0.24-0.39	501	16	7

Table 1. The table is a summary of the results of this study. n = number of graphite crystals analyzed in each sample. R2 = the interval where all the analyzed graphite crystals R2 values will land. T(°C) = maximum temperature registered from the sample. SD = standard

Discussion

Occurrence and meaning of graphite

The discussion of the petrography of the studied samples focuses on the occurrence of graphite. The analyzed samples are:

- micaschist (thirteen samples, twelve samples from the Sanfront-Pinerolo Unit and one sample from the Serre Unit)
- calcschist (two samples from the Serre Unit and one sample from the Raccias Unit)
- marble (one sample from the Serre Unit).

Micaschist and calcschist display high graphite modal amount and the samples from the Pinerolo Unit are the richest ones. In this Unit, the sample SN1902 is characterized by the highest graphite modal amount (ca. 45%).

In all samples, graphite occurs in the matrix and it is generally concentrated in layers marking the main foliation. This suggests that graphite was present before or during the development of the foliation (i.e. before or during deformation). Graphite also occurs as inclusions in several minerals, such as garnet, chloritoid, white mica, tourmaline, chlorite, albite, and carbonate. The occurrence of graphite inclusions in several minerals stable at different P-T conditions, suggests that carbonaceous material was present in the sedimentary protolith and was transformed into graphite during metamorphism.

Thermometry on carbonaceous material

Raman thermometry on carbonaceous material was applied on nine samples from the *Sanfront-Pinerolo Unit*. Eight samples (SN1902, CH2003, GM1404b, GM1405a, GM1419b, GM1406a, GM1908 and CH1902) have been collected in the northern part of the Sanfront-Pinerolo Unit, along a W-E section. No previous petrological studies have been conducted in this part of the Unit and no temperature estimates have been done so far. The maximum temperatures registered by these samples range between 531 ± 21 °C and 568 ± 17 °C.Amongst the eight analyzed samples, sample CH1902 records the highest temperature, i.e. 568 ± 17 °C. This sample has been collected relatively close to a diorite body. Therefore, the slightly highest temperature may be tentatively attributed to contact metamorphism, occurring prior to the Alpine history.

Sample PO2081 has been collected in the southern part of the Sanfront-Pinerolo Unit (close to Sanfront village) and displays a maximum temperature of 532 ± 11 °C. A recent study (Bonnet et al. 2022) conducted in the same area of the Sanfront-Pinerolo Unit investigated rutile crystals in order (i) to date the high-pressure metamorphism of this unit and (ii) to estimate the temperature registered by this unit. Rutile thermometry provides a temperature of crystallization on rutile by measuring the Zr content present in this mineral. For the Sanfront-Pinerolo Unit temperatures in the range 474-513 °C have been estimated on two samples (Bonnet et al. 2022). These values are slightly lower than the one obtained in the present study (based on Raman spectroscopy on carbonaceous material). However, it is important to keep in mind that rutile thermometry provides a crystallization temperature and this temperature can be lower than the maximum temperature reached by a rock during its metamorphic evolution. Another petrological investigation (Groppo et al. 2019) in the southern sector of the Sanfront-Pinerolo Unit, provided a maximum temperature of 510-520 °C. These values are similar to the ones obtained in this study.

To sum up, the northern and southern sector of the Sanfront-Pinerolo Unit registered the same maximum temperature within the error.

In the newly discovered *UHP Chasteiran Unit* (Manzotti et al, in press), two samples have been investigated (GM2010 and CH1907-2). Their peak temperature has been estimated at 526 ± 28 C° and 532 ± 14 °C, respectively (graph 19). These values are consistent with the one obtained by Manzotti et al. (in press) by thermodynamic modelling.

The *Serre Unit* consists of remnants of the continental Mesozoic cover of the Dora-Maira Massif. It consists of marble, calcschist and rare micaschist. Four samples (GM2004b, GM1904, GM1907 and CH2016) have been investigated in this unit. The maximum temperature registered by these samples range between 480 ± 17 C° and 513 ± 16 °C. This temperature range is within error similar to the maximum temperature recorded by the Chasteiran unit.

In the southern Dora-Maira Massif, the Cima di Crosa Unit is an equivalent of the Serre Unit. Rutile thermometry (Bonnet et al 2022) indicated a temperature of crystallization of 403 °C (graph 21). This value is significantly lower than the temperature estimated for the Serre Unit by Raman spectroscopy on carbonaceous material from this study. In this part of the Dora-Maira Massif, there are two other units similar to the Serre Unit in their lithological content, i.e. the Val Grana and the Maira Units (Michard et al. 2022). A recent study (Michard et al. 2022) investigated a set of samples in both units by Raman spectroscopy on carbonaceous material. The Val Grana Unit is characterized by a range of temperature between 370 and 510 °C and displays a clear increase of temperature from west to east (graph 20). The Maira Unit shows a maximum temperature in the range 450-510 °C and it also displays a clear increase of temperature from west to east (graph 20). The maximum temperature recorded by the Serre Unit in the northern Dora-Maira Massif are therefore similar to the temperature of the eastern sector of the Val Gran and Maira Units.

By comparing the data from the present study with the one of Michard et al. (2022), it can be noted a largest error in the data of Michard et al. (2022). This can be simply due to the fact that the authors plot the standard deviations instead of the confidence (graph 20).

The *Raccias Unit* is a thin eclogite-facies oceanic unit, cropping out on top of the continental Serre Unit. A calcschist sample (GM2029) from this Unit has been analyzed and provides a maximum temperature of 501 ± 16 °C. This value is within error similar to the one of the Serre and Chasteiran Units. The Raccias Unit should be connected to the Viso Unit to the south. For the latter, previous estimated temperatures are in the range 480-580 °C (Angiboust et al. 2012; Schwartz et al. 2000; Messiga et al. 1999; Castelli et al. 2002; Groppo et al. 2010).

Graph 19:

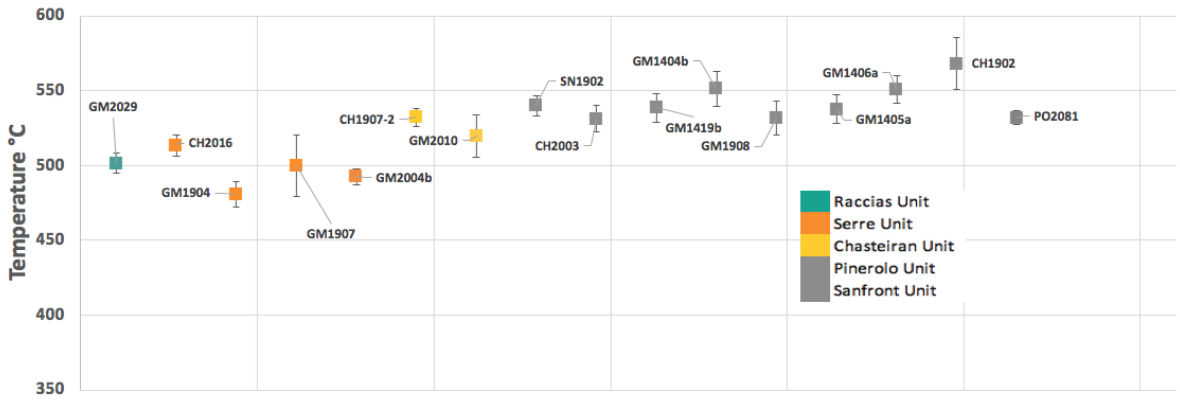

Graph 19. This Graph is the same graph as graph 17 only difference is that the temperature matching the (Michard et al 2022) to be able to compare them much easier.

Graph 20:

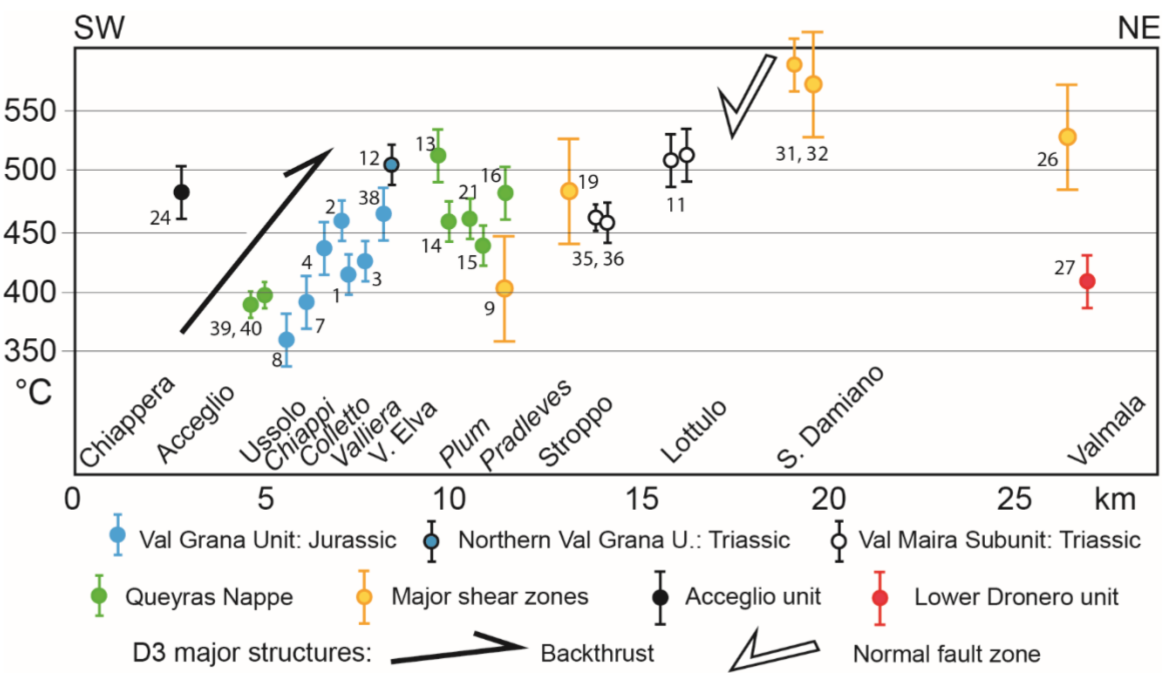

Graph 20. Graph of the Raman temperature results from the paper (Michard et al 2022).

Graph 21:

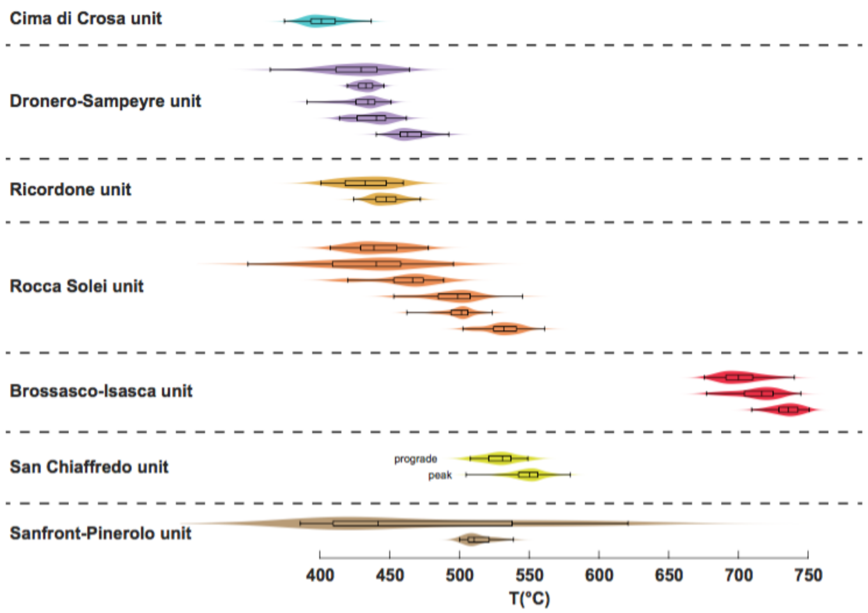

Graph 21. The graph is taken from Bonnet et al 2022 and shows temperature data on rutile.

To sum up, the data obtained in this study by Raman spectroscopy on carbonaceous material suggest that overall there is no a significant temperature difference from west to east in the northern sector of the Dora-Maira Massif (Germanasca, Chisone and Sangone vallyes). The Sanfront-Pinerolo Unit (located to the east of the studied section) registered slightly higher temperatures than the Chasteiran, Serre and Raccias Units. To fully understand this difference, further investigations are needed.

Conclusions

The main conclusions of this study are as follows:

- Raman spectroscopy on carbonaceous material conducted on sixteen samples along a west-east section across the northern Dora-Maira Massif indicates that overall there is no significant difference in the maximum temperatures (480 ± 17 °C to 551 ± 23 °C) registered within the Dora-Maira nappe stack, as.
- Slightly higher temperatures are registered by the Sanfront-Pinerolo Unit (531 ± 21 °C to 551 ± 23 °C, with an outlier at 568 ± 17 °C). The geological meaning of this difference is not fully understood and will require further investigations.
- Along the northern Dora-Maira Massif, the Mesozoic Serre Unit records a maximum temperature (480 ± 17 C° to 513 ± 16 °C) similar to the most eastern sector of the Mesozoic Val Grana and Maira Units in the southern Dora-Maira Massif.

Acknowledgment

I would like to thank my supervisor Paola Manzotti for all the guidance in the writing process and moral support but not to forget the time in the field in Italy to help me understand the basics of the Alps. A big thanks have to be given to Michel Ballèvre and Stefan M. Schmid for all the support and guidance in the field. Thank you, Francesco Nosenzo, for the support in report writing and in the field. Thanks to my co-supervisor Federica Schiavi that was helping me learn the Raman technique and also helping me in the Ramen part of the report. Last, I like to thank Vidar Jakobsson for inspiration in the report writing.

References

Angiboust, S., Agard, P., Jolivet, L., & Beyssac, O. (2009). The Zermatt-Saas ophiolite: the largest (60-km wide) and deepest (c. 70–80 km) continuous slice of oceanic lithosphere detached from a subduction zone? *Terra Nova*, *21*(3), 171-180.

Agard P. (2021). Subduction of oceanic lithosphere in the Alps: Selective and archetypal from (slow-spreading) oceans. *Earth-Science Reviews*, 214, 103517.

Agard P, Monié P, Jolivet L, Goffé B (2002) Exhumation of the Schistes Lustrés complex: in situ laser probe 40Ar/39Ar constraints and implications for the Western Alps. *Journal of Metamorphic Geology* 20:599–618.

Agard P.,Handy M.R. (2021). Ocean subduction dynamics in the Alps. *Elements*, 17, 9–16.

Ballèvre M., Camonin A., Manzotti P., Poujol M. (2020). A step towards unraveling the paleogeographic attribution of pre-Mesozoic basement complexes in the Western Alps based on U–Pb geochronology of Permian magmatism. *Swiss Journal of Geosciences*, 113:12.

Bachmann, R., Glodny, J., Oncken, O., & Seifert, W. (2009). Abandonment of the South Penninic–Austroalpine palaeosubduction zone, Central Alps, and shift from subduction erosion to accretion: constraints from Rb/Sr geochronology. *Journal of the Geological Society*, *166*(2), 217-231.

Beyssac, O., & Lazzeri, M. (2012). Application of Raman spectroscopy to the study of graphitic carbons in the Earth Sciences. *European Mineralogical Union Notes in Mineralogy*, *12*(12), 415-454.

Beyssac, O., Goffé, B., Petitet, J. P., Froigneux, E., Moreau, M., & Rouzaud, J. N. (2003). On the characterization of disordered and heterogeneous carbonaceous materials by Raman spectroscopy. *Spectrochimica Acta Part A: Molecular and Biomolecular Spectroscopy*, *59*(10), 2267-2276.

Beyssac, O., Goffé, B., Chopin, C., & Rouzaud, J. N. (2002). Raman spectra of carbonaceous material in metasediments: a new geothermometer. *Journal of metamorphic Geology*, *20*(9), 859-871.

Bounous C. (2018) Talco e grafite delle valli Chisone e Germanasca. Miniere tra storia e memoria. LAR Editore, 148 pp.

Bousquet, R., Oberhänsli, R., Goffé, B., Wiederkehr, M., Koller, F., Schmid, S.M., Schuster, R., Engi, M., Berger, A., & Martinotti, G. (2008). Metamorphism of metasediments at the scale of an orogen, a key to the Tertiary geodynamic evolution of the Alps. In: Sigesmund S., Fügenschuh B., Froitzheim N. (eds.), Tectonic Aspects of the Alpine-Dinaride-Carpathian System. *Geological Society London, Special Publication*, *298*, 393–411.

Compagnoni R., Rolfo F. (2003). UHPM units in the Western Alps. Ultrahigh-pressure units in the Western Alps. *In Carswell, D. A., Compagnoni, R. Ultrahigh-pressure metamorphism. Budapest: Eötvös University Press, European Mineralogical Union Notes in Mineralogy*, 5, 13–49.

Chopin, C. (1984). Coesite and pure pyrope in high-grade blueschists of the Western Alps: a first record and some consequences. *Contributions to Mineralogy and Petrology*, *86*(2), 107-118.

Decrausaz, T., Müntener, O., Manzotti, P., Lafay, R., & Spandler, C. (2021). Fossil oceanic core complexes in the Alps. New field, geochemical and isotopic constraints from the Tethyan Aiguilles Rouges Ophiolite (Val d'Hérens, Western Alps, Switzerland). *Swiss Journal of Geosciences*, *114*(1), 1-27.

Fenn, M. B., Xanthopoulos, P., Pyrgiotakis, G., Grobmyer, S. R., Pardalos, P. M., & Hench, L. L. (2011). Raman spectroscopy for clinical oncology. *Advances in Optical Technologies*, *2011*.

Gabalda S., Beyssac O., Jolivet L., Agard P., Chopin C. (2008). Thermal structure of a fossil subduction wedge in the Western. *Terra* Nova, 21, 28–34.

Gallach, X., Perrette, Y., Lafon, D., Chalmin, É., Deline, P., Ravanel, L., ... & Wallet, T. (2021). A new method for dating the surface exposure age of granite rock walls in the Mont Blanc massif by reflectance spectroscopy. *Quaternary Geochronology*, *64*, 101156

Gabalda, S., Beyssac, O., Jolivet, L., Agard, P., & Chopin, C. (2009). Thermal structure of a fossil subduction wedge in the Western Alps. *Terra Nova*, *21*(1), 28-34.

Gasco, I., Gattiglio, M., & Borghi, A. (2011). *Lithostratigraphic setting and P-T metamorphic evolution for the Dora Maira Massif along the Piedmont Zone boundary*. International Journal of Earth Sciences, 100, 1065–1085.

Goffé, B., Schwartz, S., Lardeaux, J.-M., & Bousquet, R. (2004). Explanatory notes to the map: Metamorphic structure of the Western Alps and Ligurian Alps. *Mitteilungen der Österreischischen Mineralogischen Gesellschaft*, *149*, 125-144.

Groppo C., Ferrando S., Gilio M., Botta S., Nosenzo F., Balestro G., Festa A., Rolfo R. (2019) What's in the sandwich? New P–T constraints for the (U)HP nappe stack of southern Dora-Maira Massif (Western Alps). *European Journal of Mineralogy*, 31, 665–683.

Handy, M. R., Schmid, S. M., Bousquet, R., Kissling, E., & Bernoulli, D. (2010). Reconciling plate-tectonic reconstructions of Alpine Tethys with the geological–geophysical record of spreading and subduction in the Alps. *Earth-Science Reviews*, 102(3-4), 121-158.

Herviou, C., Verlaguet, A., Agard, P., Locatelli, M., Raimbourg, H., Lefeuvre, B., & Dubacq, B. (2021). Along-dip variations of subduction fluids: The 30–80 km depth traverse of the Schistes Lustrés complex (Queyras-Monviso, W. Alps). *Lithos*, *394-395*, 106168.

Jannin , P., Magrì, F. (2017). Antiche miniere delle Alpi Cozie Vol. 2. Guida storica-escursionistica. Alzani Editore, 349 pp.

Keller, L. M., Hess, M., Fügenschuh, B., & Schmid, S. M. (2005). Structural and metamorphic evolution of the Camughera–Moncucco, Antrona and Monte Rosa units southwest of the Simplon line, Western Alps. E*clogae Geologicae Helvetiae*, *98*(1), 19-49.

Lagabrielle, Y., & Cannat, M. (1990). Alpine Jurassic ophiolites resemble the modern central Atlantic basement. *Geology*, *18*(4), 319-322.

Lagabrielle, Y., Brovarone, A. V., & Ildefonse, B. (2015). Fossil oceanic core complexes recognized in the blueschist metaophiolites of Western Alps and Corsica. *Earth-Science Reviews*, *141*, 1-26

Le Breton, E., Brune, S., Ustaszewski, K., Zahirovic, S., Seton, M., & Müller, R. D. (2020). Kinematics and extent of the Piemont-Liguria Basin–implications for subduction processes in the Alps. *Solid Earth Discussions*.

Manzotti, Pitra P.,Langlade J., Ballèvre M. (2015). Constraining P–T conditions during thrusting of a higher pressure unit over a lower pressure one (Gran Paradiso,Western Alps). *Journal of Metamorphic Geology,* 33, 981-1002.

Manzotti P., Ballèvre M., Poujol M. (2016) Detrital zircon geochonology in the dora-Maira and zone Houillere: a record of sediment travel paths in the Carboniferous. *Terra Nova*, 28, 279–288.

Manzotti P., Ballèvre M. (2021). Continental subduction in the Alps: from field data to kinematic models. In: *The Alpine Chain*, Wiley, XXX-XXX.

Manzotti P., Ballèvre M., Pitra P., Schivavi F. (2021). Missing lawsonite and aragonite found: P–T and fluid composition in meta-marls from the Combin Zone (Western Alps). *Contributions to Mineralogy and Petrology*.

Manzotti P., Ballèvre M., Pitra P., Putlitz B., Robyr M., Müntener O. (2020). The growth of sodic amphibole at the greenschist-to blueschist-facies transition (Dent Blanche, Western Alps): bulk-rock chemical control and thermodynamic modelling. *Journal of Petrology,* 61(4), egaa044.

Manzotti P, Schiavi F, Nosenzo F, Pitra P, Ballèvre M (2022). A journey towards the forbidden zone: a new, cold, *UHP* unit in the Dora-Maira Massif (Western Alps). Contributions to Mineralogy and Petrology, in press

Markley, M. J., Teyssier, C., Cosca, M. A., Caby, R., Hunziker, J. C., & Sartori, M. (1998). Alpine deformation and 40Ar/39Ar geochronology of synkinematic white mica in the Siviez-Mischabel Nappe, western Pennine Alps, Switzerland. *Tectonics*, *17*(3), 407-425.

McCarthy A., Tugend J., Mohn G., Candioti L., Chelle-Michou C., Arculus R., Schmalholz S., Müntener O. (2020). A case of Ampferer-type subduction and consequences for the Alps and the Pyrenees. *American Journal of Science*, 320, 313–372.

Michard, A., Avigad, D., Goffé, B., & Chopin, C. (2004). The high-pressure metamorphic front of the south Western Alps (Ubaye-Maira transect, France). *Schweizerische Mineralogische und Petrographische Mitteilungen*, *84*, 215-235.

Novarese V. (1895). Sul rilevamento eseguito nel 1894 in valle della Germanasca (Alpi Cozie). Bollettino del Reale Comitato Geologico d'Italia, 26, 253–282.

Novarese V. (1898). I giacimenti di grafite delle Alpi Cozie. Bollettino del Reale Comitato Geologico d'Italia, 29, 3–35.

Novarese V. (1905). La grafite nelle Alpi piemontesi. Atti della Accademia Reale delle Scienze di Torino, 40, 1–16.

Nosenzo, F., Manzotti, P., Poujol, M., Ballèvre, M., & Langlade, J. (2022). A window into an older orogenic cycle: P-T conditions and timing of the pre-Alpine history of the Dora-Maira Massif (Western Alps). *Journal of Metamorphic Geology*.

Pfiffner, O. A. (2014). *Geology of the Alps*. John Wiley & Sons.

Reinecke, T. (1991). Very-high-pressure metamorphism and uplift of coesite-bearing metasediments from the Zermatt-Saas zone, Western Alps. *European Journal of Mineralogy*, 7-18.

Rosenbaum, G., Lister, G. S., & Duboz, C. (2004). The Mesozoic and Cenozoic motion of Adria (central Mediterranean): a review of constraints and limitations. *Geodinamica Acta*, *17*(2), 125-139.

Schmid, S.M., & Kissling, E. (2000). The arc of the western Alps in the light of geophysical data on deep crustal structure. *Tectonics*, *19*, 62–85.

Schmid, S. M., Fügenschuh, B., Kissling, E., & Schuster R. (2004). Tectonic map and overall architecture of the Alpine orogeny. *Eclogae Geologicae Helvetiae*, 97, 93–117.

Schuster, R., & Stüwe, K. (2008). Permian metamorphic event in the Alps. *Geology*, 36, 603-606.

Sandrone R., Cadoppi P., Sacchi R., Vialon P. (1993). The Dora-maira massif. In: Pre-Mesozoic geology in the Alps. Berlin: Springer, 317–325.

Smye A.J., Seman S.M., Scambelluri M., Starr P.G., Federico L. (2021). Exhumation dynamics of high-pressure metamorphic rocks from the Voltri Unit, Western Alps: constraints from phengite Rb–Sr geochronology. *Contributions to Mineralogy and Petrology*, 176:14.

Schmid, S. M., Fügenschuh, B., Kissling, E., & Schuster, R. (2004). Tectonic map and overall architecture of the Alpine orogen. *Eclogae Geologicae Helvetiae*, *97*(1), 93-117.

Tajčmanová, L., Manzotti, P., & Alvaro, M. (2021). Under pressure: high-pressure metamorphism in the Alps. *Elements: An International Magazine of Mineralogy, Geochemistry, and Petrology*, *17*(1), 17-22.

Vialon, P. (1966) Étude géologique du massif crystalline Dora-Maira, Alpes Cottiennes Internes, Italie. PhD thesis. *Grenoble: Faculté des sciences de Grenoble*. 293 pp.

White, R. S. (1984). Atlantic oceanic crust: seismic structure of a slow-spreading ridge. *Geological Society, London, Special Publications*, *13*(1), 101-111.